Geochemistry 82 (2022) 125821

Contents lists available at ScienceDirect

Geochemistry

journal homepage: www.elsevier.com/locate/chemer

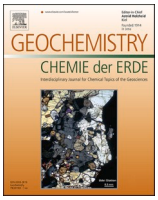

Multistage melt impregnation in Tethyan oceanic mantle: Petrochemical constraints from channelized melt flow in the Naga Hills Ophiolite

A. Verencar [a], A. Saha [a,b,*], S. Ganguly [c], M. Satyanarayanan [d], B. Doley [a,b], M. Ram Mohan [d]

[a] CSIR-National Institute of Oceanography, Dona Paula, Goa 403 004, India
[b] Academy of Scientific and Innovative Research, Ghaziabad, Uttar Pradesh 201 002, India
[c] School of Earth, Ocean and Atmospheric Sciences, Goa University, Taleigão Plateau, Goa 403 206, India
[d] CSIR-National Geophysical Research Institute, Uppal Road, Hyderabad 500 007, India

ARTICLE INFO

Handling Editor: Sanjeet Verma

Keywords:
Mantle harzburgite
Melt channel
Melt-rock interaction
Refertilisation
Boninite
Suprasubduction zone

ABSTRACT

Ophiolitic sequences obducted onto continental margins allow field based observations coupled with petrochemical interrogations of upper mantle lithologies thereby aiding evaluation of compositional heterogeneity of oceanic mantle, depletion-enrichment events and geodynamic conditions governing oceanic lithosphere formation. The Naga Hills Ophiolite (NHO) suite preserves a segment of the Neotethyan oceanic lithosphere encompassing a package of mantle and crustal lithologies. This paper for the first time reports the occurrence of melt flow channels traversing the mantle section near Molen of the NHO and presents a comprehensive study involving chromite-spinel chemistry, bulk rock major, trace and PGE geochemistry to understand the petrogenesis and evolution in a geodynamic transition from mid oceanic ridge (MOR) to suprasubduction zone (SSZ). The spinel chemistry of peridotitic melt channels depicts both MOR-type and SSZ signatures underlining a transitional tectonic frame. Chromite chemistry and high Al_2O_3/TiO_2 ranging from 15.98–35.70 in concurrence with low CaO/Al_2O_3 ranging from 0.03–0.53; and chondrite normalised LREE > MREE < HREE patterns confirm the influx of boninitic melts into the refractory mantle. The boninitic signature shared by melt channels and host rock invokes a geochemical and geodynamic transition from anhydrous melting of depleted mantle to hydrated fluid flux melting resulting in boninitic melts, that subsequently impregnate and refertilise the fore arc mantle wedge in a SSZ regime at the nascent stage of subduction. The high Ba/Nb, Ba/Th, and Ba/La for the studied peridotites highlight the influx of subduction derived fluids in the supra subduction mantle. Further higher Zr/Hf and Nd/Hf with respect to primitive mantle values in concurrence with lower Nb/Ta suggest progressive refertilisation due to fluid- and melt-driven metasomatism of the refractory fore arc mantle wedge. The chondrite normalised PGE patterns suggest positive Ir and Ru anomalies stipulating the source to be refractory while enriched Pt and Pd underpins the mobilisation of these elements by subduction derived fluids and melts. The elevated abundances of PPGEs than IPGEs as cited by PPGE/IPGE > 1; and Pd/Pt avg. 0.85 for melt channels and 0.84 for host peridotites indicate fluid-fluxed metasomatism of fore arc mantle wedge with a S-undersaturated trend coupled with boninitic affinity. The mineral, trace, REE and PGE chemistry collectively emphasizes that the mantle peridotites of the NHO formed in a transitional geodynamic tectonic setting caused by fore arc extension during subduction initiation followed by rejuvenation by subduction derived fluids and boninitic melts, which typically are of the SSZ tectonic regime. The harzburgitic melt channels and host rock are refractory in nature, reflecting multiple episodes of melt extraction of about 5–15% and ~10–20% respectively from a spinel peridotite mantle source. The occurrences of these melt channels indicate segregation and percolation of melt through porous and channelized network in upper mantle peridotites.

1. Introduction

Mantle dykes, diffused and channelized melt flows embedded within the upper mantle peridotites in ophiolitic sequences exemplify the pathways allowing melt segregation, migration and percolation at mantle-transition zone (MTZ). Mantle dykes, delineated by two distinct

* Corresponding author at: CSIR-National Institute of Oceanography, Dona Paula, Goa 403 004, India.
E-mail address: asaha@nio.org (A. Saha).

https://doi.org/10.1016/j.chemer.2021.125821
Received 18 June 2021; Received in revised form 5 September 2021; Accepted 6 September 2021
Available online 22 September 2021

parallel contacts with host harzburgites, represent the most common melt migration structures recording multi-stage magma generation processes in the evolutionary history of ophiolites (Kelemen et al., 1995). However, there are other melt migration structures that share many attributes with the mantle dykes but are porous and reactive, thereby termed as melt channels or channelized melt flows (Python and Ceuleneer, 2003).

Petrological and geochemical features of these intra mantle dykes and melt channels along with their host peridotites are marked by a complex evolutionary history comprising multiple stages of melt generation, segregation, infiltration from variable magma sources. The pristine compositions of intruding melts and host peridotites are often modified by flow segregation and assimilation reaction processes which in turn influence their petrogenetic characters. The mantle dykes are commonly affected by intense plastic deformation hindering relative sequential record of emplacement and deformation events (Python and Ceuleneer, 2003). Compositionally, these intra mantle dykes cover a wide compositional spectrum from pyroxenite (orthopyroxenite, websterite and clinopyroxenite) to boninites (Varfalvy et al., 1996, 1997; Bodinier et al., 1987, 1990; Keleman, 1990). Melt transport through upper mantle under extensional stress regime invokes segregation and percolation of melt through porous and channelized networks (Rabinowicz et al., 1987; Batanova and Savelieva, 2009). This mechanism of channelized porous flow induces pervasive interaction between the invasive melt and the host peridotite. The phenomenon of silicate melt transfer in the mantle from the site of their generation at depth to the emplacement in the crust are principally governed by two end member processes viz. (i) reactive porous flow with continuous equilibration with the peridotite and (ii) focused channelized flow with absence of equilibrium due to limited interaction of the melt with the surrounding peridotites (Kelemen et al., 1995). Melt transport processes in subduction zone environment largely differs from that in a mid-oceanic ridge (MOR) setting owing to mantle composition, partial melting conditions and the temperature at crust-mantle transition zone. Melt transport mechanisms in the sub arc mantle wedge include both reactive porous flow and focused channelized flow which yield insights into melt evolution in the oceanic sub arc mantle. The hydrous condition in the melt generation regime of an arc and the lower pressure-temperature of resultant hydrous melts generated within arc modify the crystallization sequence and melt propagation mechanism like hydraulic fracturing (Lambart et al., 2009, 2016). Thus, suprasubduction environment are characterised by melt filled fractures. Melt channels of dunitic and pyroxenitic compositions cross cutting the mantle sections of ophiolites hold significant implications for melt generation and focused melt transport in the sub arc upper mantle from 3 to 4 km below the crust-mantle transition zone. These are discordant and non-brittle features discernible in the field and their mineral and trace element chemistry suggest that these channels carry silicate melts much different in composition than that of typical N-MORB (Pirard, 2010). The mantle sections of the Naga Hills Ophiolite (NHO) are formed in supra subduction zone (SSZ) tectonic environment and record imprints of distinct multi-stage magmatic events viz. (i) a refractory mantle rendered depleted by multiple episodes of melt extraction events during fore arc extension and (ii) melt replenishment and refertilisation of this depleted mantle in response to subduction initiation and impregnation of slab-derived melts and fluids in a SSZ regime (Verencar et al., 2021). This SSZ mantle refertilisation is primarily driven by the influx of high degree, shallow level boninitic melts generated by partial melting of a metasomatized fore arc mantle wedge at the inception of oceanic subduction. This study for the first time reports the occurrence of channelized melt flows within the mantle peridotites (~host rocks) of the NHO exposed at south of Molen. We present mineral chemistry of oxide phases and bulk rock major, trace, REE and PGE data for the melt channels and host peridotites of the NHO to comprehensively address the compositional characteristics and mutual relation with their host, restitic nature, refertilisation of source mantle, melt generation and migration processes that governed the chemical evolution of the Tethyan ocean sub arc mantle.

2. Geological setting

The Naga Hills Ophiolite (NHO) belt in the Indo-Myanmar range (IMR) represents a segment of Tethyan oceanic crust and upper mantle that was involved in an eastward convergence, collision and accretion of the Indian Plate with the Eurasian Plate at the Indo-Myanmar continental margin during the Late Cretaceous-Eocene (Acharyya et al., 1989; Ghose et al., 1987). The origin and emplacement of ophiolitic rocks of IMR are debatable till date. Both subduction and non-subduction origin of these rocks have been described by several workers in recent studies (Khogenkumar et al., 2021; Singh et al., 2016). The non-subduction related mafic rocks are characterised by their high-Ti, alkaline, Ocean Island Basalts (OIB) to low-Ti MORBs with enriched LILE and HFSE concentrations while ultramafic rocks are residual products of high degree partial melting of upper mantle at a spreading zone associated with plate divergence due to initial separation of Indian Plate from Antarctica and Australia during late Jurassic to Early Cretaceous (Khogenkumar et al., 2021). The subduction related mafic rocks are tholeiitic, low–Ti, LREE and HFSE depleted in nature; high Cr chromitites and depleted dunites represent fore arc tectonic setting and were probably formed during Early Cretaceous and the beginning of Late Cretaceous (Khogenkumar et al., 2021).

The N-S trending IMR is approximately 1250 km long and lies to the south of the eastern Himalayan syntaxis and extends further south, in structural continuity with the trail of Andaman volcanic arc islands (Acharyya et al., 1990; Fig. 1a inset). The NHO belt occurs along a narrow (5–15 km wide), NNE trending and westerly convex 200 km linear belt in the northern sector of Indo-Myanmar range, consisting of four tectono-stratigraphic divisions namely (i) The Naga Metamorphic complex (ii) The Naga Hills Ophiolitic complex (iii) Inner Fold belt (iv) Belt of Schuppen; that are thrusted over each other resulting in nappes and klippes (Ghose et al., 1987; Fig. 1a). Two major thrust systems viz. Disang thrust and Haflong-Naga thrust exist in the region which form the roof and floor of the Belt of Schuppen respectively (Rao, 1983). The Penrose type NHO is emplaced as dismembered tectonic slices in the flyschoidal sediments of Disang Formation. Altogether, on the basis of structural and lithological correlation between the different thrusted slices, a complete ophiolitic sequence was reconstructed in NHO (Ghose et al., 1987; Khogenkumar et al., 2021; Singh et al., 2016; Verencar et al., 2021 and references therein). The suite comprises mantle peridotites representing upper mantle section of Tethyan oceanic lithosphere, while cumulate ultramafic-mafic rocks, pillow basalts and pelagic sediments represent the corresponding crustal sections. The ultramafic rocks include dunite, pyroxenite, and peridotites whereas the mafics include gabbro, olivine gabbro, norite and gabbro-norite along with the felsic variants represented by plagiogranites and trachytes. The mantle peridotites of NHO are exposed in and around northeast of Moki, south of the village of Molen and Weshelo, and Lacham (Verencar et al., 2021). In a road section to the north of the village of Molen (25°36.24′ N: 94°42.02′E) (Fig. 1b), occurrence of melt channels (~porous channel flow) have been noted cutting across the mantle peridotites (Fig. 2a). Probably melt channels act as pathway of melt percolation after partial melting of mantle rocks to form the crustal section. They are peridotitic in nature and highly fractured (Fig. 2b). The intensity of the serpentinisation is much higher than the serpentization observed in the host

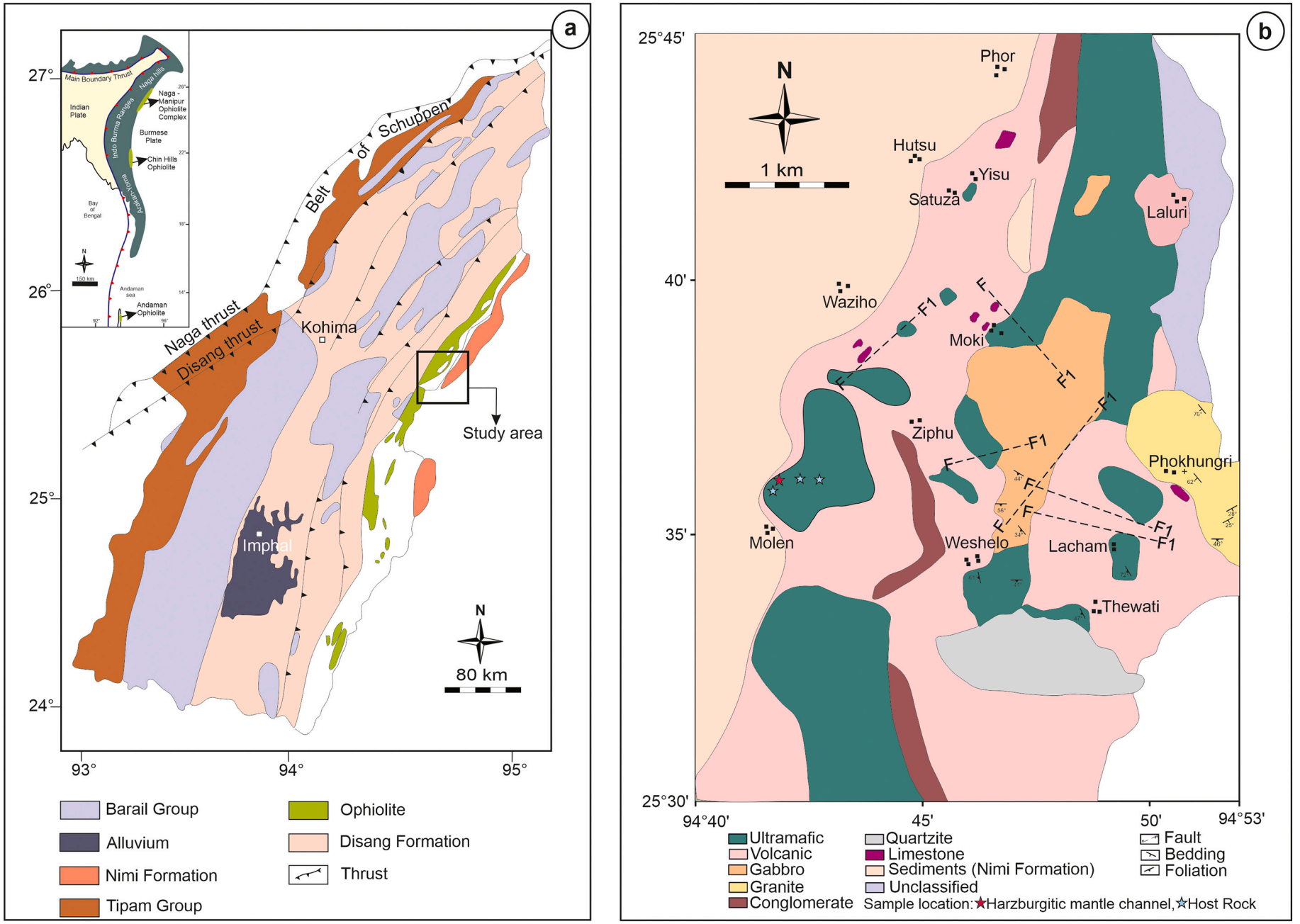

Fig. 1. (a) Simplified geological and tectonic map of Nagaland-Manipur, India (modified after Geological Survey of India and Ningthoujam et al., 2012), Inset: Simplified tectonic map of eastern margin of India depicting Naga-Manipur, Chin Hills and Andaman Ophiolitic complexes; (b) Geological map of Naga Hills ophiolite with sample locations of mantle peridotites, exposed in and around southwest of Moki, north and northeast of Molen (modified after Agrawal and Ghose, 1986).

mantle peridotites. These melt channels are irregular bodies ascribed to episodic melt migration process, channelized melt flow in a porous matrix and/or melt flow restricted in cracks. Further, the planar features within the host peridotites can be interpreted as "melt migration structures" (Python and Ceuleneer, 2003).

3. Sampling and analytical techniques

In this study, representative samples of melt channel and host rocks were collected from the village of Molen (25°36.24′ N: 94°42.02′E) (Fig. 1b). The collected host rock samples were from close proximity to the melt channels. Polished sections of the peridotites were prepared and examined under transmitted and reflected light using Nikon eclipse LV100 POL optical microscope at CSIR-National Institute of Oceanography (NIO), Goa, India. Quantitative chemical analyses of constituent mineral phases from selected thin sections of mantle peridotites were performed at CSIR-NIO, using CAMECA SX Five Electron Probe Micro Analyser operating at an acceleration voltage of 15 kV and a beam current of 10 nA. Both natural (diopside for SiO_2 and CaO; plagioclase for Al_2O_3; rutile for TiO_2; magnetite for $Fe_2O_3^T$; olivine for MgO; rhodonite for MnO, apatite for P_2O_5; albite for Na_2O; and orthoclase for K_2O) and synthetic (chromium oxide for Cr_2O_3) standards were used during the analyses. The precision of the analysis is better than 1% for major element oxides.

Fourteen relatively fresh, unweathered peridotite samples devoid of carbonate veins and surficial alteration were selected and pulverised in an agate disc mill at CSIR-NIO. These samples were analysed for major oxides, trace elements including REE and PGE concentrations along with matrix matching geochemical reference materials for quality control at CSIR-National Geophysical Research Institute (NGRI), Hyderabad, India. Major oxides concentration was determined using X-ray fluorescence spectroscopy (XRF; Phillips MAGIX PRO MODEL 2440), from pressed pellets prepared from the powdered rock samples. About 2 g of powdered samples were sprayed onto a collapsible aluminum cup of diameter 4 cm filled with boric acid and were pressed under a hydraulic press (Hydraulic Press, Herzog, Germany) at 25 ton pressure. Certified Reference Material (CRM) namely UB-N (ANRT, France) and JP-1, (GSJ, Japan) were used to estimate the accuracy of the results. The method for preparation of pellets and the protocol followed during analysis can be found elsewhere (Krishna et al., 2007). The precision of the analysis is better than 3% for major element oxides. The trace, rare earth and platinum group of elements were determined using high resolution inductively coupled mass spectrometer (HR-ICP-MS; Nu Instruments Attom®, UK) in jump-wiggle mode at CSIR-NGRI. The trace elements including rare earth elements (REE) were analysed by employing closed digestion method using HF and HNO_3 at 7:3 proportion with few drops of perchloric acid and the clear diluted solutions were analysed by HR-ICP-MS,. Certified reference material UB-N from ANRT (France), PCC-1 from USGS (USA), JP-1 from GSJ (Japan) were also treated in the same way as the samples, and used for quality control measures. ^{103}Rh was used as an internal standard. Precision and reproducibility obtained for international reference materials were found to be better than 8% RSD for majority of the trace elements. The PGEs were evaluated using nickel sulphide fire-assay pre-concentration method along with international reference materials WMG-1, WMS-1 (CANMET, Canada) and PTM-1 (IGGE, China). 10 g of the sample was thoroughly mixed with to 80 g borax, 40 g sodium carbonate, 6 g silica, 2 g nickel powder, 1.2 g sulphur powder and 1.5 g calcium fluoride; which was further transferred into a fire clay crucible and fused at 1100 °C in a muffle furnace in order to obtain a NiS button upon cooling of the melt in the iron mold. The button was then powdered and digested following the method described in Balaram et al. (2006), and analysed by HR-ICP-MS for PGEs. The detailed methodology, instrumental parameters, detection limits and data processing protocol used are after Satyanarayanan et al. (2018). The precision and reproducibility for most of the PGEs were less than 10% obtained for all reference materials used as quality control.

4. Petrography

The intrusive peridotitic melt channels have undergone pervasive and penetrative serpentinisation. In most of the places, primary mineralogy is not preserved due to pervasive influx of hydrothermal solution. Almost all olivine grains are altered to serpentine group of minerals forming secondary foliation and giving rise to a tectonic fabric. Most of the minerals are sheared and elongated in a particular direction (Fig. 3a). With further progressive deformation, the foliation is transformed to asymmetric crenulation (Fig. 3b) due to high strain at mantle depth. Orthopyroxene grains are also serpentinised but degree of alteration is lesser than the olivine grains and in some places a few grains of relict orthopyroxenes were observed (Fig. 3c). Mineralogically, these melt channel peridotites are harzburgitic in nature. Chromites and chrome spinels are the most dominant primary opaque and occur as micro-pods and inclusions in silicate minerals. Chromites are euhedral to subhedral whereas chromium bearing spinels are anhedral in shape (Fig. 3d). In some places, chromium bearing spinels show compositional zoning. The significant presence of chromium bearing oxide minerals indicate their mantle origin. Magnetites are present as an alteration product of chromite and chromium bearing spinels and are formed during post-magmatic hydrothermal activity.

The peridotitic host rock is relatively less serpentinised as compared to the peridotitic melt channels (Fig. 3e). Primary magmatic texture has been partially preserved. Mineralogically, the peridotite is harzburgitic

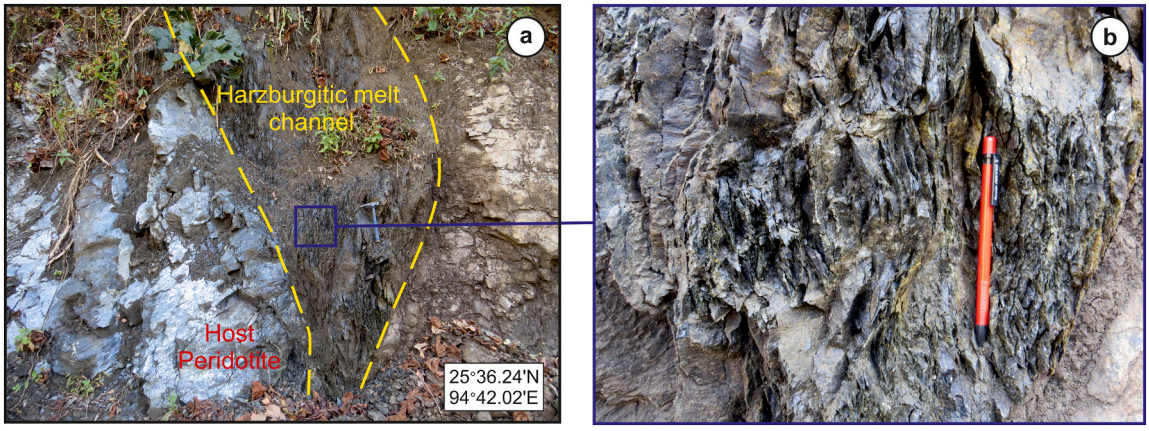

Fig. 2. (a) Field photograph of an outcrop of harzburgitic melt channel in contact with host peridotite north of Molen (b) Field photograph of sheared peridotitic melt channel (enlarge view).

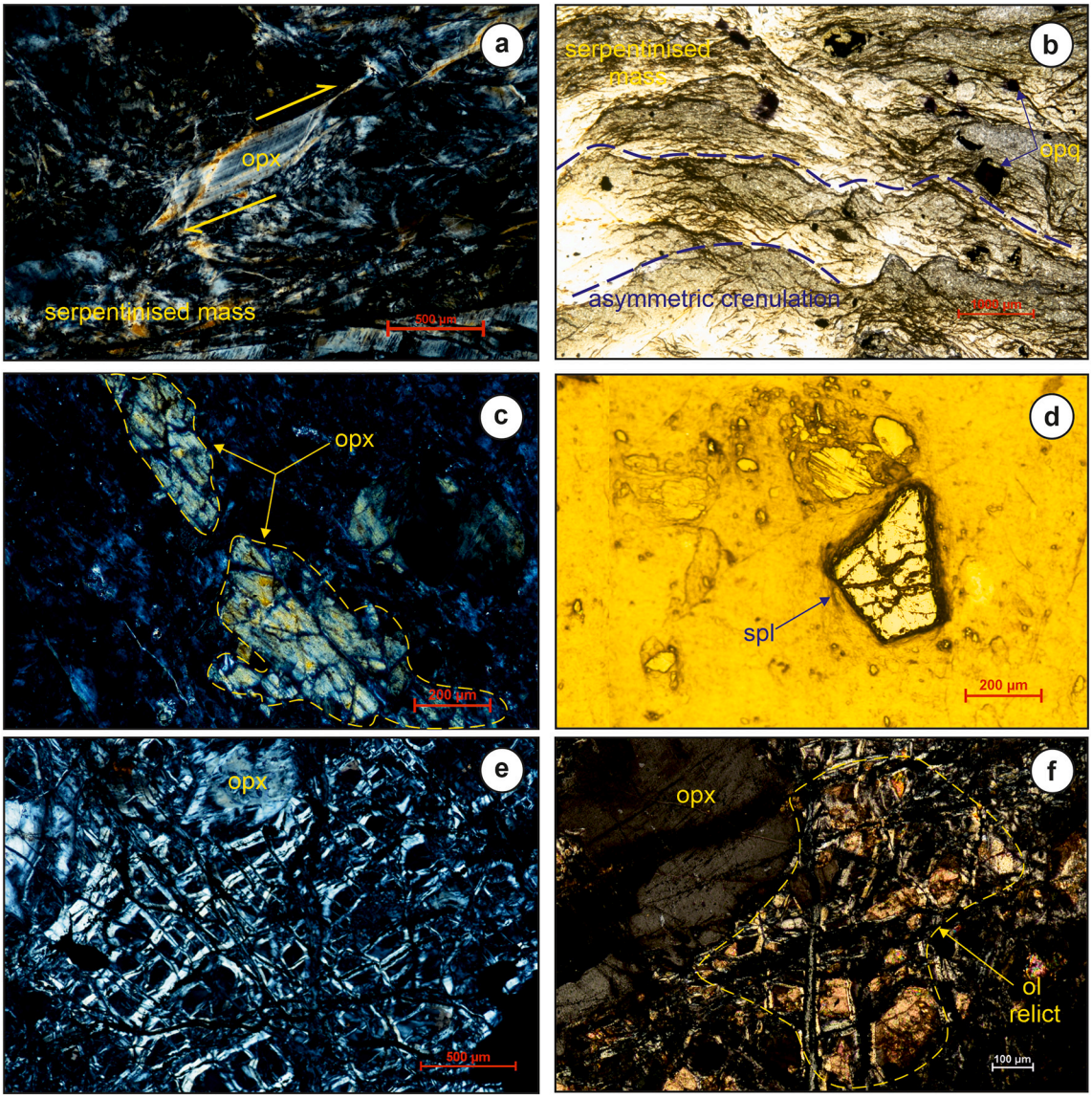

Fig. 3. Photomicrographs showing (a) the effect of shearing in a relict orthopyroxene grain in peridotitic melt channel (b) pervasive serpentinisation and development of asymmetric crenulations in peridotitic melt channel (c) the occurrences of orthopyroxene in peridotitic melt channel (d) the occurrence of primary aluminous phase-spinel in peridotitic melt channel (e) development of mesh texture due to serpentinisation in peridotitic host rock (f) occurrences of primary olivine and orthopyroxene in peridotitic host rock. Figs (a), (c), (e) and (f) have been captured in between cross polars; and Fig. (b) and (d) have been captured under plane polarized light and reflected light respectively.

on account of its dominance in modal orthopyroxenes, followed by clinopyroxenes and olivines (Fig. 3f). Olivine pseudomorphs are occasionally present in host peridotites. Presence of olivine relict is also observed. Olivine altered serpentinite grains form a typical mesh like texture with growth of thick fibrous chrysotile veins. Secondary magnetite occurs either as stringers or patches or within serpentinite veins.

5. Mineral chemistry

5.1. Primary chromium bearing aluminous phases

Based on the major element chemistry, the chromium bearing aluminous phases have been compositionally subdivided into chromite and chrome spinel (Table 1) found in the melt channels. Chromites are characterised by high Cr_2O_3 (54.42–55.36 wt%), moderate Al_2O_3 (10.75–11.74 wt%), $Fe_2O_3^T$ (23.85–25.23 wt%) and MgO (7.78–8.65 wt %). Chrome spinels are showing a compositional range of relatively lower Cr_2O_3 (27.27–36.64 wt%), higher Al_2O_3 (27.13–38.73 wt%), $Fe_2O_3^T$ (15.94–25.85 wt%), low MgO (12.08–16.55 wt%) than chromites (Supplementary Table S1). Cr# values vary from 0.76–0.77 and 0.32–0.46 and Mg# values range from 0.40–0.44 and 0.56–0.74 for chromites and chrome spinel respectively. Cr/Fe^{2+} values for both the phases are >1 (chromites: 2.50–2.65 and chrome spinel: 1.74–2.87) indicating early partitioning of Cr with respect to other mafic ions from an ultramafic magma (Supplementary Table S1). These characteristics are similar to that of primary mantle chromian spinels with minimal post-compositional change (Arai et al., 2006; Kharbish, 2020). In the Cr-Al-Fe^{3+} discrimination diagram, chromite grains show their compositional range from Fe-chromite to Al-chromite and fall very close to the boninitic field. In the spinel classification diagram chrome spinels are showing their picotitic nature as expected in ophiolitic spinels (Fig. 4a).

Table 1
Major oxides, trace element (including REE and PGE) concentrations of the studied rocks.

	Melt channel				
	ML161	ML162	ML163	ML164	ML165
wt%					
SiO_2	37.26	36.66	39.03	40.07	38.68
TiO_2	0.09	0.08	0.05	0.03	0.06
Al_2O_3	1.85	1.38	1.13	0.76	1.01
$Fe_2O_3^T$	12.47	10.60	12.95	10.30	10.50
MnO	0.11	0.11	0.10	0.08	0.09
MgO	33.60	35.55	32.24	34.16	34.80
CaO	0.15	0.11	0.09	0.07	0.17
Na_2O	0.09	0.07	0.08	0.07	0.09
K_2O	0.01	0.01	0.01	0.01	0.02
P_2O_5	0.04	0.04	0.04	0.04	0.04
LOI	14.88	14.48	14.80	14.97	14.84
Sum	100.54	99.09	100.52	100.57	100.30
Mg#	70	74	68	74	74
ppm					
Cr	2391	2127	2257	2802	1963
Co	83.23	84.45	84.68	105.28	63.23
Ni	2034	1934	2048	2628	1618
Rb	3.82	2.02	1.61	1.64	1.80
Sr	10.05	7.40	6.32	6.34	5.55
Cs	0.65	1.13	0.75	0.71	0.55
Ba	32	17	15	15	13
Sc	13	11	9	10	8
V	54	43	39	38	37
Ta	0.01	0.01	0.01	0.01	0.01
Nb	0.14	0.06	0.05	0.05	0.09
Zr	3.36	3.22	3.09	3.74	3.40
Hf	0.08	0.08	0.07	0.08	0.07
Th	0.06	0.04	0.03	0.03	0.03
U	0.10	0.07	0.11	0.05	0.04
Y	2.84	2.09	2.01	2.29	2.23
La	0.47	0.28	0.33	0.30	0.29
Ce	1.13	0.66	0.81	0.72	0.72
Pr	0.15	0.09	0.11	0.10	0.10
Nd	0.78	0.45	0.55	0.52	0.51
Sm	0.25	0.16	0.18	0.18	0.18
Eu	0.12	0.10	0.10	0.11	0.10
Gd	0.38	0.25	0.27	0.28	0.26
Tb	0.07	0.05	0.05	0.05	0.05
Dy	0.47	0.35	0.32	0.36	0.33
Ho	0.11	0.08	0.07	0.08	0.07
Er	0.31	0.24	0.21	0.24	0.19
Tm	0.05	0.04	0.03	0.03	0.03
Yb	0.32	0.25	0.22	0.23	0.20
Lu	0.05	0.04	0.03	0.03	0.03
∑REE	4.65	3.04	3.29	3.24	3.07
Cu	37	24	22	26	22
Pb	32	28	21	36	12
Ga	4.02	3.27	3.40	3.89	3.28
ppb					
Ru	12.10	12.11	9.03	11.45	12.21
Rh	1.09	1.02	0.76	0.91	1.07
Pd	23.97	21.87	12.63	13.36	18.22
Ir	15.04	14.15	11.42	14.82	15.24
Pt	26.57	23.82	15.15	18.15	20.63
∑PGE	78.77	72.96	48.99	58.69	67.36
∑IPGE	27.14	26.26	20.44	26.27	27.45
∑PPGE	51.63	46.70	28.54	32.43	39.91
Al_2O_3/TiO_2	20.73	17.91	21.73	27.25	15.98
CaO/Al_2O_3	0.08	0.08	0.08	0.10	0.17
$(La/Sm)_N$	1.22	1.17	1.18	1.07	1.07
$(Gd/Yb)_N$	1.00	0.83	0.99	1.04	1.06
$(La/Yb)_N$	1.06	0.80	1.07	0.97	1.04
Nb_N	0.56	0.26	0.20	0.21	0.36
Th_N	2.16	1.43	1.15	1.19	0.98
$(Ta/La)_{PM}$	0.36	0.36	0.30	0.33	0.29
$(Hf/Sm)_{PM}$	0.45	0.70	0.56	0.64	0.60
Eu/Eu*	1.14	1.47	1.41	1.53	1.44
Ba/Th	508.95	417.99	440.53	438.44	475.81
Ba/La	68.05	61.51	44.33	49.93	46.33
Ba/Nb	229.97	275.31	306.19	293.30	153.16
Dy/Yb	1.49	1.40	1.46	1.58	1.65

(*continued on next page*)

Table 1 (*continued*)

	Melt channel				
	ML161	ML162	ML163	ML164	ML165
Gd/Lu	8.30	6.86	8.01	9.00	8.70
La/Yb	1.48	1.12	1.49	1.35	1.45
Nb/Ta	13.85	10.52	8.01	8.63	17.57
Nb/U	1.35	0.90	0.45	1.05	2.10
Nd/Hf	10.13	5.91	7.67	6.26	7.04
Nb/Yb	0.44	0.25	0.22	0.23	0.44
Th/Nb	0.02	0.01	0.01	0.01	0.01
Th/Yb	0.20	0.17	0.15	0.15	0.14
Zr/Hf	43.58	42.73	43.18	45.37	46.55
Zr/Nb	24.25	50.98	64.30	72.23	38.70
∑PPGE/∑IPGE	1.90	1.78	1.40	1.23	1.45
Pt/Pt*	3.22	3.13	3.02	3.22	2.89
Cu/Ir	2445	1664	1971	1735	1462
Cu/Pd	1534	1077	1782	1924	1223
Cu/Pt	1384	989	1484	1416	1080
Ni/Cu	55.32	82.10	91.05	102.24	72.66
Ni/Pd	84,874	88,409	162,211	196,720	88,845
Pd/Ir	1.59	1.55	1.11	0.90	1.20
Pd/Pt	0.90	0.92	0.83	0.74	0.88
Pt/Pd	1.11	1.09	1.20	1.36	1.13
$(Pt/Ir)_N$	0.80	0.76	0.60	0.55	0.61
$(Pd/Ir)_N$	1.32	1.28	0.92	0.75	0.99

	Melt channel				Host rock	
	ML166	ML167	ML168	NG214	ML158	ML159
wt%						
SiO_2	41.25	38.51	39.00	41.58	37.43	38.92
TiO_2	0.05	0.05	0.06	0.04	0.06	0.03
Al_2O_3	0.98	1.03	1.14	0.96	1.63	1.07
$Fe_2O_3^T$	9.34	12.47	12.10	9.26	7.06	7.85
MnO	0.09	0.09	0.09	0.09	0.12	0.07
MgO	33.13	33.03	33.42	34.20	39.31	37.24
CaO	0.09	0.11	0.10	0.08	1.91	0.03
Na_2O	0.05	0.08	0.09	0.05	0.04	0.01
K_2O	0.01	0.01	0.02	0.01	0.01	0.01
P_2O_5	0.04	0.04	0.04	0.04	0.04	0.04
LOI	14.92	14.85	14.87	14.62	12.85	14.12
Sum	99.93	100.26	100.94	100.93	100.46	99.40
Mg#	75	70	70	76	83	80
ppm						
Cr	595	1787	5287	2156	2364	2158
Co	13.56	51.82	145.33	77.18	80.92	78.44
Ni	199	1293	3932	1888	1818	1789
Rb	2.95	1.41	2.45	1.92	2.11	1.80
Sr	8.03	5.81	8.82	5.59	8.02	6.16
Cs	0.17	0.55	1.25	0.72	0.14	0.11
Ba	24	15	27	18	15	15
Sc	6	6	16	8	13	9
V	14	27	66	37	58	44
Ta	0.01	0.01	0.01	0.00	0.01	0.01
Nb	0.03	0.05	0.30	0.05	0.03	0.03
Zr	1.40	2.60	4.85	2.69	2.48	2.27
Hf	0.03	0.06	0.11	0.06	0.06	0.05
Th	0.04	0.03	0.08	0.02	0.04	0.05
U	0.05	0.07	0.08	0.05	0.08	0.08
Y	1.96	1.76	3.26	1.46	2.11	1.09
La	0.29	0.28	0.56	0.21	0.25	0.23
Ce	0.69	0.65	1.33	0.49	0.60	0.53
Pr	0.10	0.09	0.18	0.07	0.08	0.07
Nd	0.50	0.44	0.92	0.33	0.40	0.33
Sm	0.17	0.14	0.29	0.12	0.13	0.10
Eu	0.11	0.10	0.18	0.08	0.06	0.04
Gd	0.25	0.20	0.43	0.18	0.23	0.14
Tb	0.05	0.04	0.07	0.03	0.05	0.03
Dy	0.31	0.26	0.50	0.21	0.34	0.19
Ho	0.07	0.06	0.11	0.05	0.08	0.05
Er	0.19	0.17	0.32	0.14	0.23	0.14
Tm	0.03	0.03	0.05	0.02	0.04	0.02
Yb	0.19	0.18	0.32	0.16	0.26	0.15
Lu	0.03	0.03	0.05	0.02	0.04	0.02
∑REE	2.99	2.65	5.30	2.11	2.80	2.02
Cu	15	18	33	21	31	29

(*continued on next page*)

Table 1 (*continued*)

	Melt channel				Host rock	
	ML166	ML167	ML168	NG214	ML158	ML159
Pb	20	27	25	20	23	20
Ga	2.43	3.03	6.21	2.92	2.24	1.67
ppb						
Ru	9.95	12.27	8.94	14.36	11.33	8.82
Rh	0.90	1.01	0.95	1.20	1.10	0.88
Pd	15.31	16.78	13.59	19.19	22.80	17.87
Ir	14.10	14.03	11.27	16.04	12.29	9.56
Pt	17.07	19.77	18.24	21.75	25.45	16.89
∑PGE	57.33	63.85	53.00	72.53	72.96	54.02
∑IPGE	24.05	26.30	20.21	30.40	23.62	18.38
∑PPGE	33.28	37.56	32.79	42.14	49.34	35.64
Al_2O_3/TiO_2	21.67	20.18	17.80	25.13	29.14	35.70
CaO/Al_2O_3	0.09	0.10	0.09	0.08	1.17	0.03
$(La/Sm)_N$	1.07	1.24	1.25	1.16	1.25	1.50
$(Gd/Yb)_N$	1.08	0.92	1.10	0.91	0.73	0.75
$(La/Yb)_N$	1.06	1.12	1.24	0.93	0.68	1.09
Nb_N	0.13	0.22	1.22	0.22	0.11	0.11
Th_N	1.45	1.11	2.67	0.86	1.54	1.63
$(Ta/La)_{PM}$	0.35	0.30	0.36	0.32	0.40	0.44
$(Hf/Sm)_{PM}$	0.28	0.58	0.56	0.78	0.70	0.79
Eu/Eu*	1.54	1.76	1.55	1.79	1.06	1.03
Ba/Th	561.73	470.34	350.93	731.19	331.70	307.33
Ba/La	82.31	55.13	48.70	87.17	59.43	63.09
Ba/Nb	739.81	283.72	90.61	336.80	563.70	522.25
Dy/Yb	1.62	1.48	1.54	1.30	1.30	1.26
Gd/Lu	9.12	7.47	9.19	7.13	5.74	6.11
La/Yb	1.48	1.56	1.73	1.30	0.94	1.53
Nb/Ta	5.34	10.69	25.02	13.48	4.38	4.63
Nb/U	0.70	0.76	3.65	1.09	0.33	0.34
Nd/Hf	15.08	7.54	8.15	5.24	6.27	6.09
Nb/Yb	0.16	0.30	0.93	0.34	0.10	0.18
Th/Nb	0.03	0.01	0.02	0.01	0.02	0.02
Th/Yb	0.22	0.18	0.24	0.16	0.17	0.31
Zr/Hf	41.88	44.54	43.12	42.86	39.41	41.79
Zr/Nb	43.60	48.62	16.16	49.79	94.47	81.60
∑PPGE/∑IPGE	1.38	1.43	1.62	1.39	2.09	1.94
Pt/Pt*	2.84	2.97	3.13	2.81	3.14	2.64
Cu/Ir	1098	1291	2891	1292	2558	2983
Cu/Pd	1011	1079	2398	1080	1379	1595
Cu/Pt	907	916	1787	953	1235	1688
Ni/Cu	12.89	71.39	120.66	91.12	57.83	62.77
Ni/Pd	13,026	77,058	289,332	98,397	79,737	100,126
Pd/Ir	1.09	1.20	1.21	1.20	1.86	1.87
Pd/Pt	0.90	0.85	0.75	0.88	0.90	1.06
Pt/Pd	1.11	1.18	1.34	1.13	1.12	0.95
$(Pt/Ir)_N$	0.55	0.63	0.73	0.61	0.93	0.80
$(Pd/Ir)_N$	0.90	0.99	1.00	0.99	1.54	1.55

	Host rock		
	ML160	ML169	ML170
wt%			
SiO_2	35.50	38.56	40.08
TiO_2	0.11	0.05	0.04
Al_2O_3	1.81	1.52	1.03
$Fe_2O_3^T$	8.07	8.98	8.43
MnO	0.07	0.08	0.14
MgO	40.75	37.31	34.90
CaO	0.51	0.15	0.55
Na_2O	0.07	0.03	0.07
K_2O	0.02	0.01	0.02
P_2O_5	0.04	0.04	0.04
LOI	12.77	13.63	15.35
Sum	99.71	100.36	100.64
Mg#	81	78	78
ppm			
Cr	3176	2214	2786
Co	113.20	78.22	74.36
Ni	3160	1835	1697
Rb	1.97	1.89	2.06
Sr	7.26	8.76	7.55
Cs	0.08	0.31	0.11

(*continued on next page*)

Table 1 (*continued*)

	Host rock		
	ML160	ML169	ML170
Ba	13	21	16
Sc	7	13	9
V	50	62	48
Ta	0.26	0.01	0.01
Nb	0.05	0.03	0.03
Zr	2.69	2.40	2.69
Hf	0.06	0.06	0.06
Th	0.09	0.04	0.03
U	0.05	0.06	0.06
Y	0.70	1.61	1.22
La	0.23	0.22	0.29
Ce	0.51	0.51	0.70
Pr	0.07	0.07	0.10
Nd	0.30	0.33	0.49
Sm	0.09	0.11	0.15
Eu	0.03	0.06	0.06
Gd	0.10	0.17	0.18
Tb	0.02	0.04	0.03
Dy	0.11	0.24	0.21
Ho	0.03	0.06	0.05
Er	0.07	0.17	0.14
Tm	0.01	0.03	0.02
Yb	0.07	0.20	0.16
Lu	0.01	0.03	0.03
∑REE	1.65	2.22	2.60
Cu	27	28	25
Pb	23	19	21
Ga	2.00	1.74	2.39
ppb			
Ru	10.49	12.98	20.46
Rh	0.97	1.31	1.38
Pd	21.19	26.13	16.21
Ir	11.54	17.01	22.57
Pt	22.25	33.51	31.46
∑PGE	66.44	90.94	92.09
∑IPGE	22.03	29.99	43.03
∑PPGE	44.41	60.94	49.06
Al_2O_3/TiO_2	17.07	28.19	28.69
CaO/Al_2O_3	0.28	0.10	0.53
$(La/Sm)_N$	1.73	1.33	1.21
$(Gd/Yb)_N$	1.17	0.69	0.92
$(La/Yb)_N$	2.30	0.78	1.27
Nb_N	0.20	0.14	0.14
Th_N	3.27	1.22	1.00
$(Ta/La)_{PM}$	18.41	0.38	0.29
$(Hf/Sm)_{PM}$	1.02	0.79	0.54
Eu/Eu*	0.99	1.27	1.09
Ba/Th	134.82	600.57	555.15
Ba/La	54.89	96.68	56.17
Ba/Nb	257.89	615.57	466.76
Dy/Yb	1.52	1.21	1.33
Gd/Lu	9.97	5.29	7.10
La/Yb	3.21	1.09	1.77
Nb/Ta	0.19	6.89	6.87
Nb/U	0.93	0.54	0.59
Nd/Hf	4.85	5.60	8.54
Nb/Yb	0.68	0.17	0.21
Th/Nb	0.04	0.01	0.01
Th/Yb	1.31	0.18	0.18
Zr/Hf	43.54	40.97	47.08
Zr/Nb	54.15	69.76	78.30
∑PPGE/∑IPGE	2.02	2.03	1.14
Pt/Pt*	3.04	3.55	4.11
Cu/Ir	2336	1631	1119
Cu/Pd	1272	1062	1558
Cu/Pt	1212	828	803
Ni/Cu	117.20	66.12	67.20
Ni/Pd	149,122	70,217	104,698
Pd/Ir	1.84	1.54	0.72
Pd/Pt	0.95	0.78	0.52
Pt/Pd	1.05	1.28	1.94
$(Pt/Ir)_N$	0.87	0.89	0.63
$(Pd/Ir)_N$	1.52	1.27	0.59

Normalisation values for REE and trace are from Sun and Mc Donough (1989); and for PGE are from McDonough and Sun (1995); Mg# = $100Mg/(Mg + Fe^{2+})$.

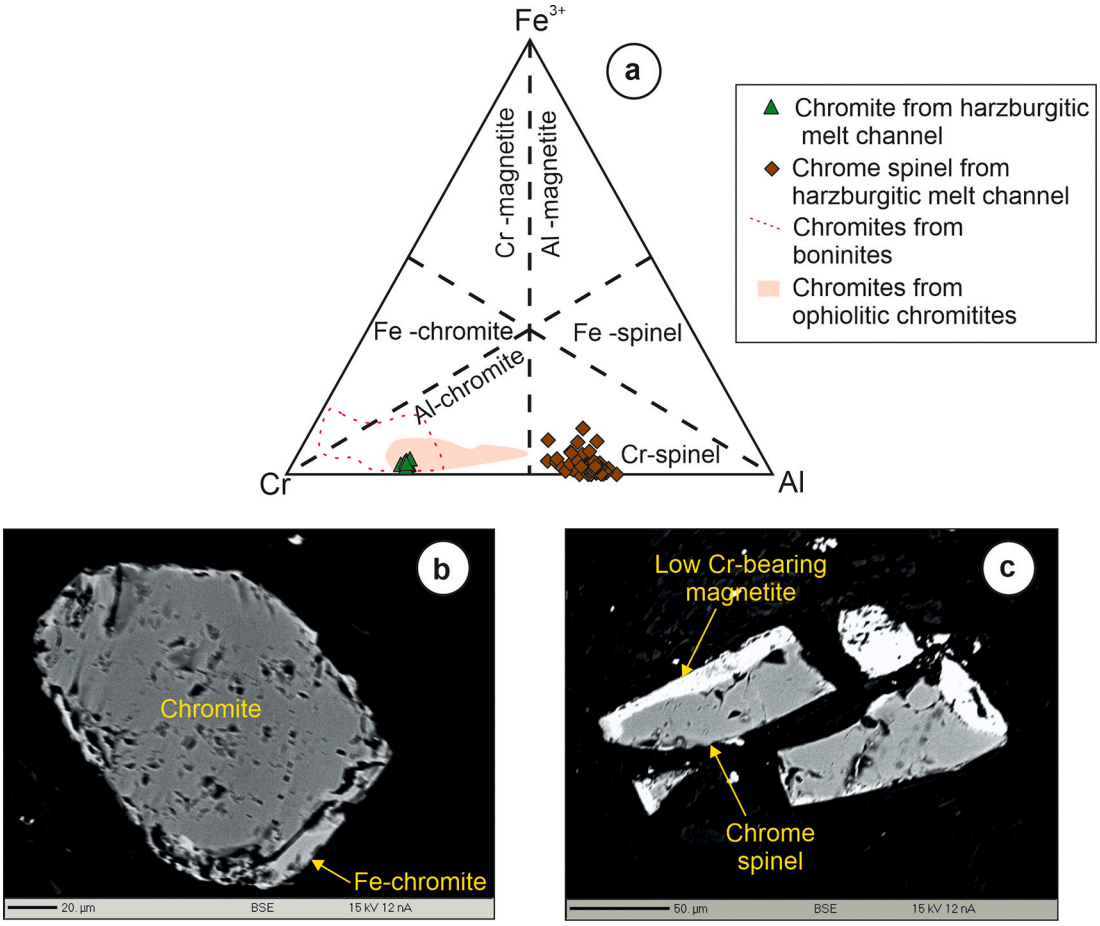

Fig. 4. (a) Trivalent Al-Fe^{3+}-Cr ternary cationic plot of spinels and chromites from peridotitic melt channel after Stevens (1944). Fields are from Barnes and Roeder (2001) (b) Back scattered electron (BSE) image of chromite and ferrian chromite in harzburgitic melt channel (c) BSE image depicting alteration of chrome spinel to low chromium magnetite in harzburgitic melt channel.

These variations in the chemistry of chromite and spinel are possibly due to varying extent of refractory nature and melt-rock interaction. The spinel chemistry further suggests that these phases are restitic after late stage melt-rock reaction and reflect equilibrium with melt compositions that are commonly associated with hydrous remelting and refertilisation in the mantle wedge above a subduction zone/supra subduction zone (Dick and Bullen, 1984).

5.2. Secondary oxide phases

Sub-solidus re-equilibration and/or ferritchromitisation during cooling, metamorphism, serpentinisation and secondary oxidation are identified as the potential factors for changing the primary chemistry of chromites (Eales and Reynolds, 1986; Lord et al., 2004). Change in chemistry of chromite and chrome spinel and extent of replacement between Cr and Fe depend on the degree of infiltration of hydrothermal fluids and alteration. In host peridotites, some of the chromite grains are altered to ferric chromite during post-magmatic alteration (Fig. 4b). The analysed ferric chromites are characterised by relatively, low Al_2O_3 and MgO concentrations (2.25–3.37 and 3.62–5.82 wt% respectively) and relatively higher Cr_2O_3 (53.68–58.18 wt%) and $Fe_2O_3^T$ (33.89–37.39 wt %) in comparison with chromite grains (Supplementary Table S2).

Chromium bearing magnetites have been formed possibly at the expense of chrome spinel grains (Fig. 4c). In the studied host peridotites, rims of the chrome spinels are showing a composition towards chromium bearing magnetites and magnetites indicating variable degree of alteration. Chromium bearing magnetites are characterised by relatively higher Cr_2O_3 (8.75–15.81 wt%) and lower $Fe_2O_3^T$ (74.00–88.03 wt%) compared to magnetites (Cr_2O_3: 0.32–3.07 wt% and $Fe_2O_3^T$:86.29–98.00 wt%) (Supplementary Table S2).

6. Geochemistry

6.1. Major oxides

Major and trace element compositions of fourteen peridotite samples are presented in Table 1. The studied peridotitic melt channels are harzburgitic in composition with low SiO_2 (36.66–41.58 wt%), TiO_2 (0.03–0.09 wt%), Al_2O_3 (0.76–1.85 wt%), CaO (0.07–0.17 wt%); moderate $Fe_2O_3^{(T)}$ (9.26–12.95 wt%) and high MgO (32.24–35.55 wt%) concentrations (Table 1). Their Mg# varies from 68 to 76. Higher loss on ignition (LOI) values for these rocks (14.48–14.97 wt%) suggests post-magmatic alteration by the influx of late stage hydrothermal fluids. The total alkali ranges from 0.06 to 0.11 wt%. These high MgO peridotitic melt channel rocks are further characterised by low CaO/Al_2O_3 (0.08 to 0.17; avg.:0.1) and high Al_2O_3/TiO_2 (15.98–27.25; avg.: 20.93) showing affinity towards Type 2 low-Ca boninites (Crawford et al., 1989). Higher proportion of normative olivine (29.18–50.54 wt%), hypersthene (25.91–49.04 wt%) with minimal plagioclase (0.56–1.34 wt%) attest their origin from a harzburgitic magma. (Supplementary Table S3).

The studied host peridotites are characterised by a restricted range of SiO_2 (35.50–40.08 wt%), TiO_2 (0.03–0.11 wt%), Al_2O_3 (1.03–1.81 wt %), CaO (0.03–1.91 wt%); lower $Fe_2O_3^{(T)}$ (7.06–8.98 wt%) and higher

MgO (34.90–40.75 wt%) than melt channels (Table 1). The total alkali ranges from 0.02 to 0.09 wt%. Their Mg# varies from 78 to 83. The studied host peridotites are having high loss on ignition (LOI) values (12.77–15.35 wt%). CaO/Al_2O_3 and Al_2O_3/TiO_2 are ranging from 0.03 to 1.17 (avg. 0.42) and 17.07–35.70 (avg. 27.76) respectively. The CIPW normative composition represents relatively high olivine (40.26–71.07 wt%), hypersthene (7.31–37.06 wt%), low proportion of plagioclase (0.08–4.58 wt%) with extremely low normative diopside in few samples (ML 158 and ML 170) (Supplementary Table S3). The high normative olivine and hypersthene proportion implies their harzburgitic nature (Supplementary Table S3). The compositional ranges of major oxide data of the studied melt channels and host rocks in terms of MgO, SiO_2, Al_2O_3 and $Fe_2O_3^{(T)}$ are very much correlatable with the compositions of the other suprasubduction zone harzburgites (Supplementary Fig. S1).

6.2. Trace elements (including rare earth elements)

The transition element chemistry for harzburgitic melt channels is characterised by enriched Cr (1787–5287 ppm, avg. 2596 ppm), Ni (1293–3932 ppm, avg. 2172 ppm) and Co (52–145 ppm, avg. 87 ppm); except for ML166 (Cr: 595 ppm, Ni: 199 ppm and Co: 14 ppm; Table 1). The total rare earth element concentration (∑REE) varies from 2.11–5.30 ppm which is much lesser than that of primitive mantle and N-MORB composition (7.43 ppm and 39.11 ppm respectively; Sun and Mc Donough, 1989). The chondrite normalised REE pattern depicts diminutive REE fractionation with positive Eu anomaly (Eu/Eu*: 1.14–1.79; Fig. 5a). LREE enrichment over MREE and HREE and MREE enrichment over HREE are marked by $(La/Sm)_N$ (1.07–1.25, LREE/MREE), $(La/Yb)_N$ (0.80–1.24, LREE/HREE) and $(Gd/Yb)_N$ (0.83–1.10, MREE/HREE) respectively. Primitive mantle normalised trace element patterns exhibit positive U, Rb, Ba and negative anomalies at Th, Ta, Nb, Hf, Zr and Ti corroborating a subduction zone origin (Fig. 5b).

The concentrations of transition elements for host peridotitic rocks reflect a higher values for Cr (2158–3176 ppm, avg. 2540 ppm), Ni (1697–3160 ppm, avg. 2060 ppm) and Co (74–113 ppm, avg. 85 ppm) (Table 1). The total REE (∑REE: 1.65–2.80 ppm) is moderately less as compared to peridotitic melt channels, primitive mantle and N-MORB (harzburgitic melt channels: 2.11–5.30 ppm; primitive mantle: 7.43 and N-MORB: 39.11 ppm; Sun and Mc Donough, 1989). The chondrite normalised REE pattern distantly resembles U-shape (Fig. 5c) and marked by $(La/Sm)_N$ (1.21–1.73, LREE/MREE), $(La/Yb)_N$ (0.68–2.30, LREE/HREE) and $(Gd/Yb)_N$ (0.69–0.92, MREE/HREE except ML160 1.17) (Table 1) collectively suggesting LREE/MREE and MREE/HREE fractionation in the source magma. Primitive mantle-normalised trace element abundance patterns display positive U, Rb, Ba and negative Th, Ta, Nb, Hf, Zr and Ti anomalies (Fig. 5d) thereby conforming to subduction-related relative LILE enrichment and HFSE depletion.

6.3. Platinum group of elements (PGEs)

The harzburgitic melt channels contain high PGE concentrations (48.99–78.77 ppb). The IPGEs range from 20.21–30.40 ppb (Ir: 11.27–16.04 ppb, Ru: 8.94–14.36 ppb), while the PPGE varies from 28.54–51.63 ppb (Pd: 12.63–23.97 ppb, Pt: 15.15–26.57 ppb and Rh: 0.76–1.20) (Table 1). These rocks are characterised by their comparable ∑PPGE/∑IPGE (>1; 1.23–1.90, avg. 1.51) and Pd/Pt (0.74–0.92, avg. 0.85) with primitive mantle (∑PPGE/IPGE: 1.85 and Pd/Pt: 0.93, Becker et al., 2006) and higher ∑PPGE/∑IPGE and Pd/Pt with respect to mid oceanic ridge peridotite (∑PPGE/∑IPGE: 1.07 and Pd/Pt: 0.84 Salters and Stracke, 2004). Pd/Ir resembles nearly chondritic values (average 1.23; C-1: 1.2, McDonough and Sun, 1995). Chondrite normalised PGE patterns display relative enrichment in Ir, Ru, Pt, Pd and depletion in Rh (Fig. 6a). The associated host peridotites are marked by higher PGE concentrations (54.02–92.09 ppb, Table 1). ∑PPGE shows relatively higher concentrations (∑PPGE: 35.64–60.94 ppb; Pd: 16.21–26.13 ppb, Pt: 16.89–33.51 ppb and Rh: 0.88–1.38 ppb) than ∑IPGE (∑IPGE: 18.38–43.03 ppb; Ir: 9.56–22.57 ppb, Ru: 8.82–20.46 ppb) in the studied peridotites. The variation in ∑PPGE/∑IPGE (1.14–2.09) and Pd/Pt (0.52–1.06) are in the range of primitive mantle values (∑PPGE/∑IPGE: 1.85 and Pd/Pt: 0.93; Becker et al., 2006). Chondrite-normalised PGE patterns are characterised by relative enrichment in Ir, Ru, Pt, Pd and depletion in Rh (Fig. 6b). Chondrite-normalised PGE patterns for the studied harzburgitic melt channels and host peridotites are consistent with that of primitive mantle and mantle peridotites from Andaman and Manipur ophiolites thereby attesting to their mantle origin (Fig. 6a and b).

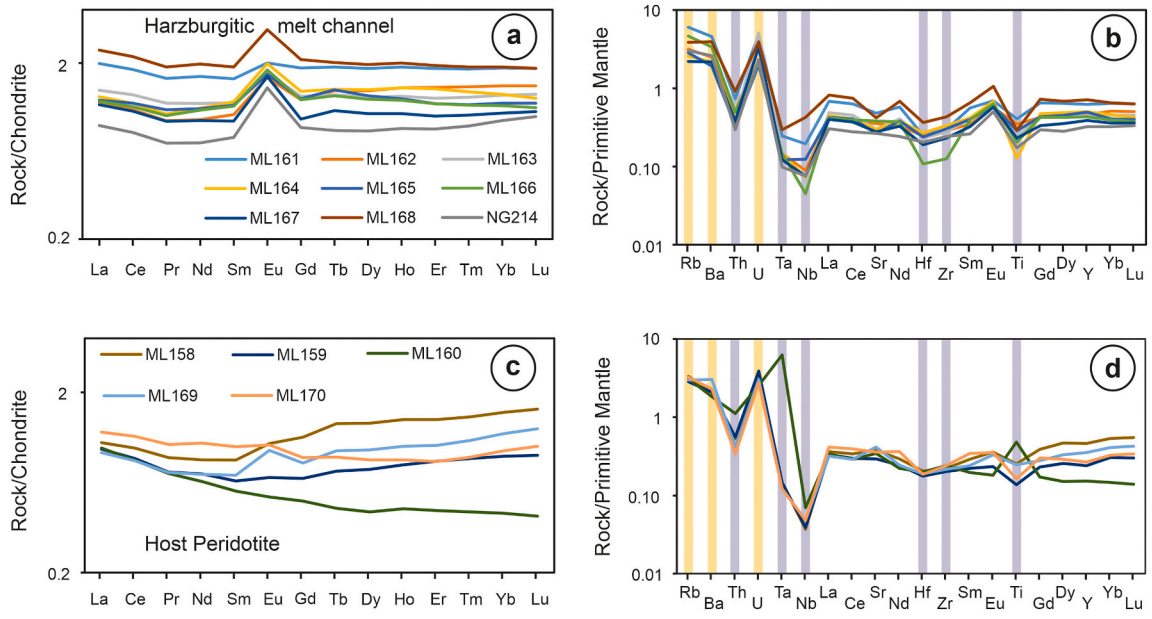

Fig. 5. Chondrite normalised REE and primitive mantle normalised REE patterns for harzburgitic melt channel and peridotitic host rock. Normalising factors are from Sun and Mc Donough (1989).

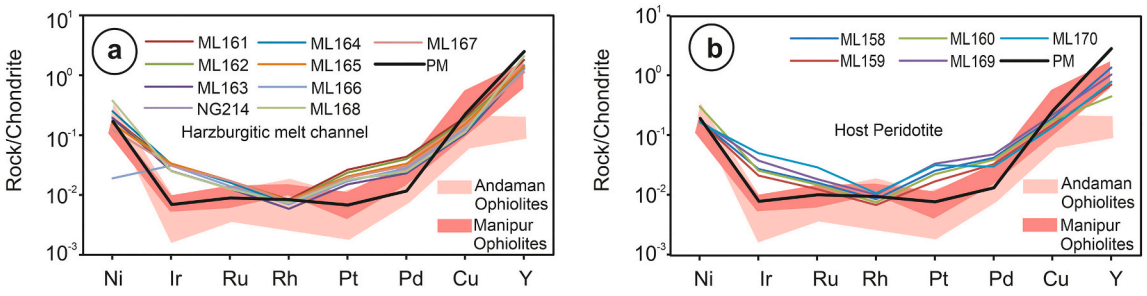

Fig. 6. Chondrite normalised PGE patterns for harzburgitic melt channel and peridotitic host rock. Normalising factors are from McDonough and Sun (1995). PGE data of primitive mantle data is from Becker et al., 2006. Fields of peridotites from Andaman ophiolites after Saha et al. (2018) and Manipur ophiolites after Singh et al. (2013).

7. Discussion

7.1. Elements screening for alteration and mobility

The complex thermo-tectonic history of peridotitic rocks from ophiolite sequences involves extensive redistribution of elements through time via various processes, starting from their formation, emplacement and subsequent accretion onto the continental margins and thereafter. Post-magmatic processes like hydrothermal alterations, metamorphism and related deformation, late stage intrusions, metasomatic alterations, and carbonation are most common to peridotitic rocks (Bodinier and Godard, 2003; Deschamps et al., 2013; Xu et al., 2020; Bhat et al., 2021), which can overprint the pristine geochemical signatures. Hence, identification of the primary geochemical signatures is a prerequisite to deliniate their petrogenesis and geodynamic implications. Chemistry of primary minerals is one of the most reliable proxies to understand the genesis and parent melt characters. Several studies have demonstrated that major elements like Al, Ti, Fe, P, high field strength elements (HFSE), REEs (except Eu and Ce) and transition metals like Cr, Ni, Sc, V and Y are relatively immobile during hydrothermal alteration and greenschist to amphibolite grade metamorphism (Laflèche et al., 1992; Arndt, 1994; Said et al., 2010). Bulk major oxide chemistry of the peridotitic protolith remains unchanged by serpentinisation and low grade metamorphism (Deschamps et al., 2013). Peltonen et al. (1998) demonstrated that transition metals like Sc, V, Cr, Co, Ni are concentrated in early crystallizing mineral phases in the magma and suffer minimal fractionation thereby preserving protolith signatures in serpentinised peridotites. Considering all these facts, primary mineral chemistry; some of the major oxides, HFSEs, transition metals and REE chemistry of bulk rocks are primarily used in this study to understand the petrogenetic processes and tectonic settings of harzburigitic melt channels and host rocks of the NHO. None of the elements is showing any linear relationship with increasing LOI content of the studied serpentinised peridotite nullifying element mobility with the post-magmatic serpentinisation processes. PGE chemistry of the bulk rocks is also taken into consideration for understanding the magmatic processes since IPGEs are refractory in their behavior, overall PPGE/IPPGE differentiation are controlled by primary partial melting conditions, degree of melt percolation, metasomatic processes in the mantle and are unaffected by post-magmatic alterations (Manikyamba and Saha, 2014).

7.2. Source characteristics: depletion-enrichment trend

Ophiolites comprise mantle and crustal sequences of relict oceanic lithosphere which record ubiquitous evidence of diverse magmatic processes and geodynamic conditions associated with its evolution from inception at MOR to termination at subduction zone. The mantle rocks particularly preserve restitic signatures rendered by episodic melt extraction events which in turn primarily attribute to the oceanic crust formation. However, the refractory mantle section of oceanic lithosphere is often modified and refertilised by (i) plume derived melts (ii) subduction derived fluids and/or melts; and (iii) recycled lithospheric components collectively endorsing pervasive geochemical heterogeneity of the oceanic mantle. The phenomenon of mantle refertilisation involves a distinct transitional magmatic regime marked by migration and impregnation of enriched melts that eventually overprint the depleted mantle character. It has been envisaged that the geochemical compositions of ophiolitic mantle rocks yield important perspectives on the magmatic and tectonic evolution of oceanic lithosphere, transitional from mid oceanic ridge (MOR) to supra subduction zone (SSZ) regime. The progressive influx of fluids and melts released through dehydration and partial melting of the subducting slab respectively into the ambient mantle wedge during initial, intermediate and mature stages of subduction, followed by slab rollback, tearing, break off and asthenospheric upwelling further modify the mantle wedge and chemical composition of the resultant melts. Primary igneous phases like chromites and chromian spinels are sensitive petrogenetic indicators that are competent in constraining the parental melt character and distinct stages of mantle evolution. (Dick and Bullen, 1984; Arai, 1994; Kepezhinskas et al., 1993; Zhou et al., 1996; Kamenetsky et al., 2001; Rollinson, 2008; Saccani and Tassinari, 2015). In this study, the chromites and chrome spinels from the harzburgitic melt channels of the NHO have Cr#: 0.76–0.77 and 0.32–0.46 respectively (Table 1) with low TiO_2 values (0.03–0.2 wt%, avg. 0.12 wt% and 0–0.29 wt%, avg. 0.08) respectively (Table 1) which are similar to the spinel compositions of depleted harzburgites of BirTuluhah ophiolites, Muğla ophiolites, SW Turkey (Abuamarah et al., 2020; Uysal et al., 2012); thereby indicating high degrees of partial melt extraction leaving behind a depleted to highly depleted residue. The Cr# values (>0.30) discernable in the studied melt channels suggest progressive melt enrichment in the source (Birner et al., 2021). In the Cr# vs. TiO_2 diagram (Fig. 7a), the chrome spinels correspond to the melt depleted domain while the chromites correspond to boninite field indicating a gradual enrichment in the source mantle. The Cr# values of chrome spinels for the melt channels (Cr#: <0.60) classify them as Type I peridotites thereby corroborating a transitional MOR environment (Dick and Bullen, 1984). This feature is substantiated in terms of TiO_2 vs Al_2O_3 variations (Fig. 7b) where the spinel compositions of the harzburgitic melt channels occupy the overlapping MORB and SSZ domain attesting to a transitional tectonic affinity. The CIPW normative olivine, hypersthene and lack of normative diopside (except in ML-158 diopside: 3.90 wt%; Supplementary Table S3) supplements a depleted refractory mantle source (Saha et al., 2018). The refractory character of studied mantle harzburgites encompassing the melt channels and the host is further reflected by relative enrichment in transitional elements viz. Cr, Ni and Mg# analogous to SSZ peridotites (Bhat et al., 2021; Bodinier and Godard, 2003; Xu et al., 2020; Table 1). The Mg# values for the melt channels (68–76) and host peridotites (78–83) are greater than 65 and are relatively higher than that of natural primitive MORB glasses. This feature is characteristic of subduction related magmas derived from re-melting of refractory

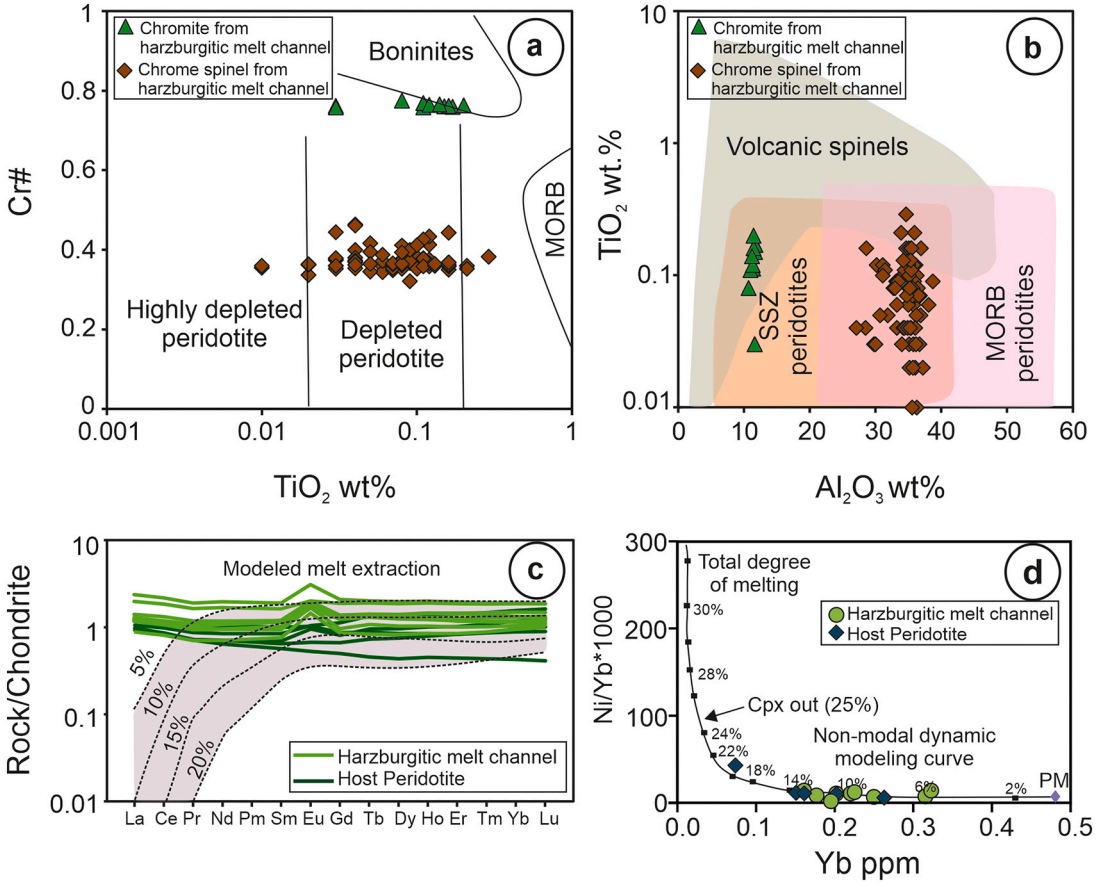

Fig. 7. (a) Cr# vs. TiO_2 wt% discrimination diagram of chromites and chrome spinels of harzburgitic melt channel after Dick and Bullen (1984); Jan and Windley (1990) and Arai (1992) (b) Binary plot of TiO_2wt% vs. Al_2O_3 wt% for chromites and chrome spinels of peridotitic host rock. Field after Kamenetsky et al. (2001) (c) chondrite normalised REE patterns for peridotitic melt channel and host rock. Fields taken from Aldanmaz and Koprubasi (2006) (d) Ni/Yb × 1000 vs. Yb ppm variation diagram for the bulk-rock chemistry of the studied mantle peridotites. Melting curve suggested by Palme and O'Neill, 2003.

mantle wedge source that has been hydrated and enriched by influx of subduction components (Varfalvy et al., 1997). Ni abundances in these melt channels (1293–3932 ppm) and host peridotites (1697–3160 ppm) are not typical of mid oceanic ridges (Ni ~ 200 ppm; Varfalvy et al., 1997) and are consistent with that observed in island arc tholeiites, back arc tholeiites, subduction related magnesian quartz tholeiites, high magnesian andesites and boninites. The high Ni and Cr contents and Mg# for the studied melt channels in conjunction with the similarity of their geochemical attributes to that of the host peridotites corroborate their generation by re-melting of a depleted restitic mantle harzburgite/lherzolite. The high Mg# and Ni contents coupled with a restitic nature suggest magma generation in a SSZ setting. The elevated transitional trace element concentrations are in agreement with shallow level hydrous mantle melting compared to those produced by anhydrous mantle peridotites. Further, chondrite-normalised REE patterns invoke a refractory source composition that experienced ~5–15% of melt extraction for the channelised melt flows and ~10–20% retrieval of melt from the source for the host peridotites (Fig. 7c). In cognizance to this, the melting model (Palme and O'Neill, 2003) based on primitive mantle spinel lherzolite mineralogy ($Ol_{0.53(-0.06)}$ + $Opx_{0.27(0.28)}$ + $Cpx_{0.17(0.67)}$ + $Sp_{0.03(0.11)}$) complies with 6% to 14% melt extraction from a spinel lherzolite mantle for the studied samples (Fig. 7d). A multi-stage melt generation process marked by ~25–>40% melt extraction from MORB-related pyrolite has been propounded for the lherzolites and harzburgites from North Arm Mountain Massif, Newfoundland (Varfalvy et al., 1997).

The siderophile Iridium-group PGEs (IPGE) are more refractory than the chalcophile Palladium-group PGE (PPGEs). Amongst the chalcophile PGEs, Pt is part of the heavy triad along with Os and Ir (Buchanan, 1988). High concentrations of IPGEs are interpreted to be residues left after high degrees of melt extraction and are often hosted in discrete minerals or sulphides within silicate grains (Rëhkamper et al., 1999; Lorand et al., 2000). The mantle harzburgites (both melt channels and host rock) in this study reflect high concentration of IPGEs (20.21–30.40 ppb avg. 25.39 ppb for melt channels and 18.38–43.03 ppb avg. 27.41 ppb for host rocks) with respect to primitive mantle and MOR peridotite values (primitive mantle: 7.5 ppb and MOR peridotites: 11.6, Becker et al., 2006; Salters and Stracke, 2004). This relatively high concentration of IPGEs underlines the source to be highly refractory. The chondrite normalised PGE diagram (Fig. 6a and b) suggests positive anomalies with respect to IPGEs (Ir and Ru) indicating the mantle peridotites to be of a more restitic nature as compared to the mantle peridotites from south Andaman ophiolitic suite (Saha et al., 2018) and Manipur ophiolitic complex (Singh et al., 2013). Xu et al. (2020) followed the PGE modelling proposed by Marchesi et al. (2013) in order to understand fractionation of PGE, partial melting and metasomatism. The model incorporated fractionation indices PPGE/IPGE i.e. Pd/Ir and Pt/Ir along with a depletion index i.e. bulk rock Al_2O_3 in order to calculate melt extraction and fractional melting curves. The $(Pt/Ir)_N$ vs. $(Pd/Ir)_N$ and $(Pt/Ir)_N$ vs. Al_2O_3 depict a distinct melt depletion trend for the studied mantle peridotites (Fig. 8a and b). The high Cr# in chromites and chrome spinels are in harmony with chromite fractionation of PGE as seen in the Cu/Ir and Ni/Pd diagram of Barnes et al. (1988) (Fig. 8c). Thus PGE fractionation in this study can be interpreted to be dominantly controlled by olivine-chromite/chrome spinel fractionation. In the Pd/Ir vs. Ni/Cu diagram, the studied samples plot in the field of refractory

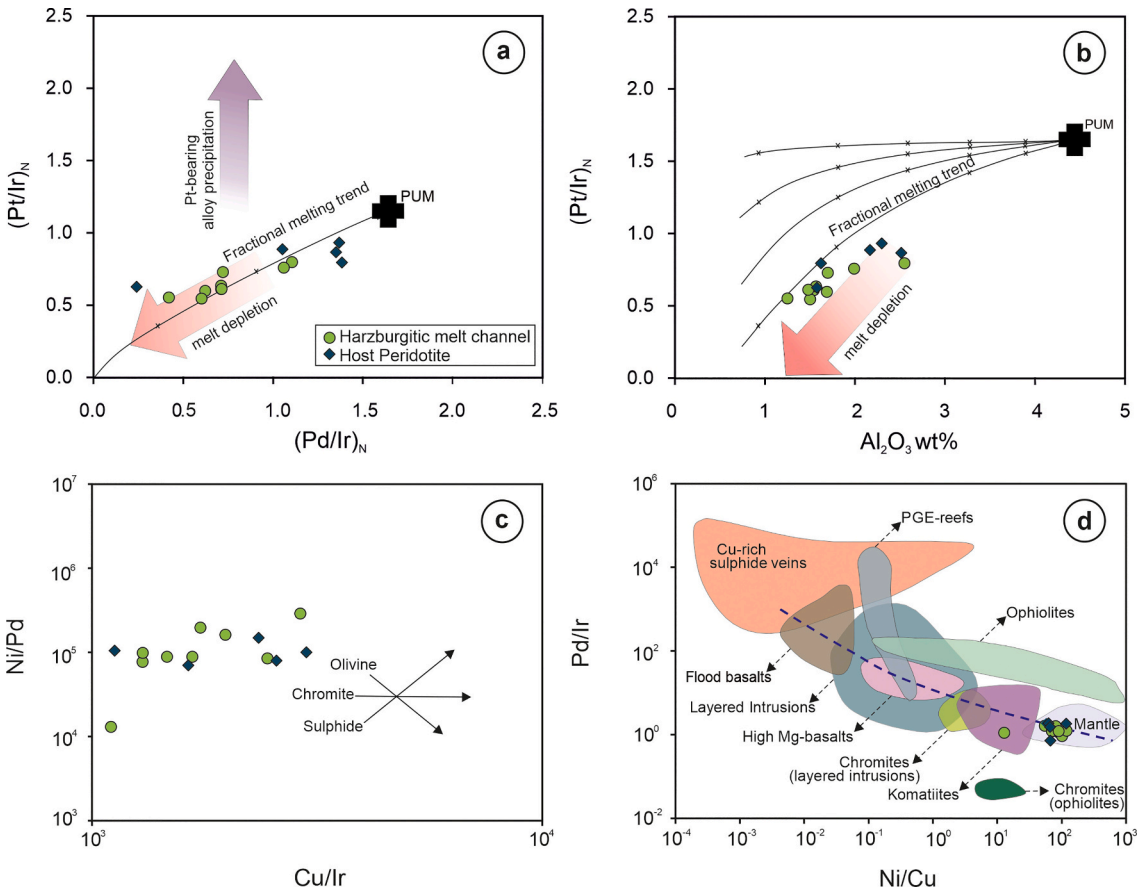

Fig. 8. (a) Whole-rock $(Pd/Ir)_N$ vs. $(Pt/Ir)_N$, and (b) $(Pd/Ir)_N$ vs. Al_2O_3wt% for peridotitic melt channel and host rock. Fields after Xu et al. (2020) and Marchesi et al. (2013) (c) Ni/Pd vs. Cu/Ir diagram of Barnes (1990) for melt channels and host rock showing chromite, olivine and sulphide fractionation trend (d) Pd/Ir vs. Ni/Cu plot of Barnes (1990) for harzburgitic melt channels.

mantle following the trend of Garuti et al. (1997) (Fig. 8d). This depletion may be translated in terms of high degrees of melt extraction leaving behind a more residual mantle as also seen in the case of Andaman ophiolitic suite (Saha et al., 2018), Manipur ophiolitic complex (Singh et al., 2013) and peridotites of Shergol and Suru Valley Ophiolites, Ladakh (Bhat et al., 2021). The low Pd/Ir ratio ranging from 0.90–1.59 for the melt channels and 0.71–1.87 for host mantle peridotites indicates high degrees of partial melting and melt extraction resulting in concentration of IPGEs in the refractory peridotites.

7.3. Boninitisation and mantle refertilisation

A conventional Penrose-type ophiolitic sequence comprises lithospheric mantle section i.e. peridotitic mantle tectonites and a crustal section which includes ultramafic-mafic cumulates, basalts and deep sea pelagic sediments (Dilek and Furnes, 2011). The crustal sections are modified by a number of factors like crustal assimilation superseding melt generation; whereas the mantle sections are more unmediating subjects in apprehending the transformation of the oceanic lithosphere in terms of its formation, modification and accretion through time (Liu et al., 2019; Xu et al., 2020; Wang et al., 2021). Studies on mantle sections have revealed the compositional heterogeneity in terms of their geochemical and isotopic distribution at different scales (O'Driscoll et al., 2012; Rampone and Hofmann, 2012; Wang et al., 2021). This is attributed dominantly to various degrees of partial melting processes and/or melt extraction occurring at various depths resulting in mantle peridotites to be more residual in origin (Choi et al., 2008; Dilek and Morishita, 2009; Niu et al., 1997). However, chemistry of primary mineral phases and whole rock geochemical signatures of relatively refractory elements designate these peridotites to deviate from its residual nature. Fluid/melt-rock and fluid/melt mantle interactions refertilise the depleted mantle restites either by percolation of sulphide melt or by impregnation of silicate melts (Luguet et al., 2003; Becker et al., 2006; Fischer-Gödde et al., 2011). Therefore, processes like melt impregnation, melt-rock and/or fluid-rock interaction, refertilisation and lithospheric recycling are accredited to the heterogeneity in the mantle (Kelemen et al., 1992; Uysal et al., 2007, 2012; Choi et al., 2008; Rampone et al., 2008; Aldanmaz et al., 2009; Rudnick and Walker, 2009; Lorand et al., 2013; Wang et al., 2021).

In the present study, the melt channels cutting across the mantle section presumably evidence the alley for infiltration and percolation of melts. Primary chromite and chrome spinel chemistry are the robust proxies useful in comprehending the processes involved in the evolution of magmatic system such as extent of partial melting/melt extraction, the role of fluids and the prevailing oxidation state in the system (Ohara et al., 2002; Rollinson, 2008; Uysal et al., 2012; Abuamarah, 2020). The chrome spinels having low Cr# (0.32–0.46) and TiO_2 (0–0.29 wt% avg. 0.08) plot in the abyssal peridotite field while the chromites having higher Cr# (0.76–0.77) and TiO_2 (0.03–0.2 wt% avg. 0.12 wt%) trend in the boninitic field (Fig. 9a). This can be explained by a reaction where spinels that formed in MOR-type environment were modified by boninitic melts during the course of melt-rock interaction resulting into chromite formation. A similar trend is seen in the chrome spinels of Muğla harzburgites and chromitites (Uysal et al., 2012). The Fe-Cr-Al ternary diagram after Stevens (1944) and Cr# vs. TiO_2 variations attest to the boninitic affinity of the chromites of the harzburgitic melt channels (Figs. 4a and 7a). This is well supported by their chrome spinel chemistry congregating in an overlapping field of SSZ and MOR type

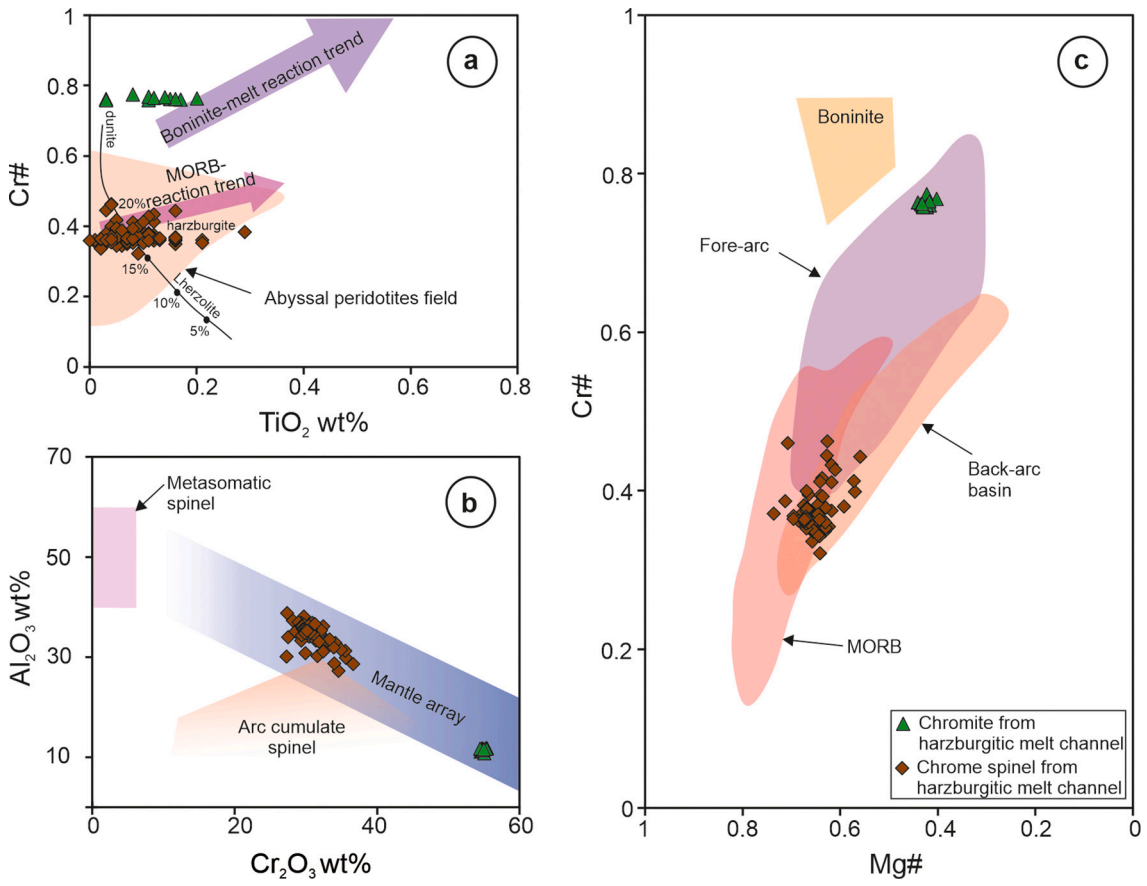

Fig. 9. (a) Cr# vs. TiO_2 wt% for chromites and chrome spinels from harzburgitic melt channels depicting boninitic and MORB-reaction trend . Fields depicting trends of different melt reactions are after Choi et al. (2008) (b) Al_2O_3 wt% vs. Cr_2O_3 wt% diagram for chromites and chrome spinels from harzburgitic melt channels showing a mantle array. Fields after Franz and Wirth (2000) (c) Cr# vs. Mg# for chromites and chrome spinels from harzburgitic melt channels indicating a transitional tectonic setting. Fields adopted from Stern et al. (2004).

peridotites in the TiO_2 vs. Al_2O_3 diagram (Fig. 7b) (Bloomer et al., 1995; Dick and Bullen, 1984; Ohara et al., 2002). The studied chromites and chrome spinels with high Cr_2O_3 and relatively low Al_2O_3 trend within the mantle array on binary plot of Al_2O_3 vs. Cr_2O_3 of Franz and Wirth (2000) (Fig. 9b). Peridotites can be distinguished into different tectonic environments based on their chromium and magnesium composition, more specifically Cr# and Mg# (Dick and Bullen, 1984; Ohara and Ishii, 1998; Barnes and Roeder, 2001; Ohara et al., 2002; Stern et al., 2004; Ali et al., 2019). In the Cr# vs Mg# diagram the chromites from the melt channels plot in the field of fore arc peridotites while the chromian spinels of the host rock largely cluster in a region overlapped by MOR-fore arc peridotites (Fig. 9c) testifying the geodynamic transition.

In general, boninitic signatures in magmas stipulate juvenile stage of intraoceanic subduction distinguished by onset of slab dehydration, fluid influx and mantle wedge metasomatism (Beccaluva et al., 2004; Dilek et al., 2008; Verencar et al., 2021). The melt channel samples plot in the overlapping field of IAT-boninites and backarc basin basalts corroborating increasing input of subduction component in a supra-subduction zone tectonic setting in the Th_N vs. Nb_N diagram (Fig. 10a). Further, the V variations with respect to Ti for the studied samples indicate a boninitic affinity (Fig. 10b). In terms of Dy/Yb vs. La/Yb variations, the studied melt channel and host rock samples fall in the spinel peridotite facies domain (Fig. 10c). This can be equated with melt generation from a garnet-free source reflecting a shallow level partial melting of peridotite consisting of olivine, orthopyroxenes, clinopyroxenes and an aluminous phase that varies with depth, in this case spinel at 0.9–3 Ga (Kepezhinskas et al., 2002; Dale et al., 2008; Saha et al., 2015).

Aqueous fluids released from the dehydrating subducting oceanic slab and hydrous melts from subducted sediments penetrate and impregnate the mantle wedge with relatively mobile elements such as LILE and LREE respectively that modify the chemistry of the resulting melts with progressive subduction at fore arc regime. The role of fluids is well pronounced in terms of LILE abundances on primitive mantle normalised trace element diagram, while chondrite normalised REE patterns depicting relative enrichment of LREE indicate role of subduction-derived melts. In the studied mantle peridotites, the LREE and HREE enrichment over MREE as rendered by LREE/MREE, LREE/HREE and MREE/HREE [$(La/Sm)_N$: 1.07–1.25, LREE/MREE, $(La/Yb)_N$: 0.80–1.24 and $(Gd/Yb)_N$: 0.83–1.10] respectively for peridotitic melt channels and [$(La/Sm)_N$: 1.21–1.73, LREE/MREE, $(La/Yb)_N$: 0.68–2.30 and $(Gd/Yb)_N$: 0.69–0.92] for the host; exemplifies a complex multi-stage petrogenetic process involving extensive melt extraction leaving behind a depleted refractory residue followed by refertilisation of the residue by percolation of boninitic melts derived through high degree shallow level melting thereby metasomatising the fore-arc mantle wedge at initial stage of subduction. This depleted to enriched compositional spectrum substantively manifests a tectonic transition from MOR to SSZ with onset of subduction and development of hydrated fore arc mantle regime. The LREE > MREE < HREE patterns for the studied rocks are comparable with South Andaman ophiolites (Saha et al., 2018), Zhangbo ophiolite from Yarlung-Zhangbo suture zone (Dai et al., 2011), the Antalya and the Ortaca ophiolite in southwestern Turkey (Uysal et al., 2007; Aldanmaz et al., 2009), the Sapat peridotite in Kohistan, northwestern Pakistan (Bouilhol et al., 2009), the Othris and the Kallidromon ophiolite in Greece (Karipi et al., 2006; Barth et al., 2008), the Khoy ophiolite in northwestern Iran (Monsef et al., 2010), the

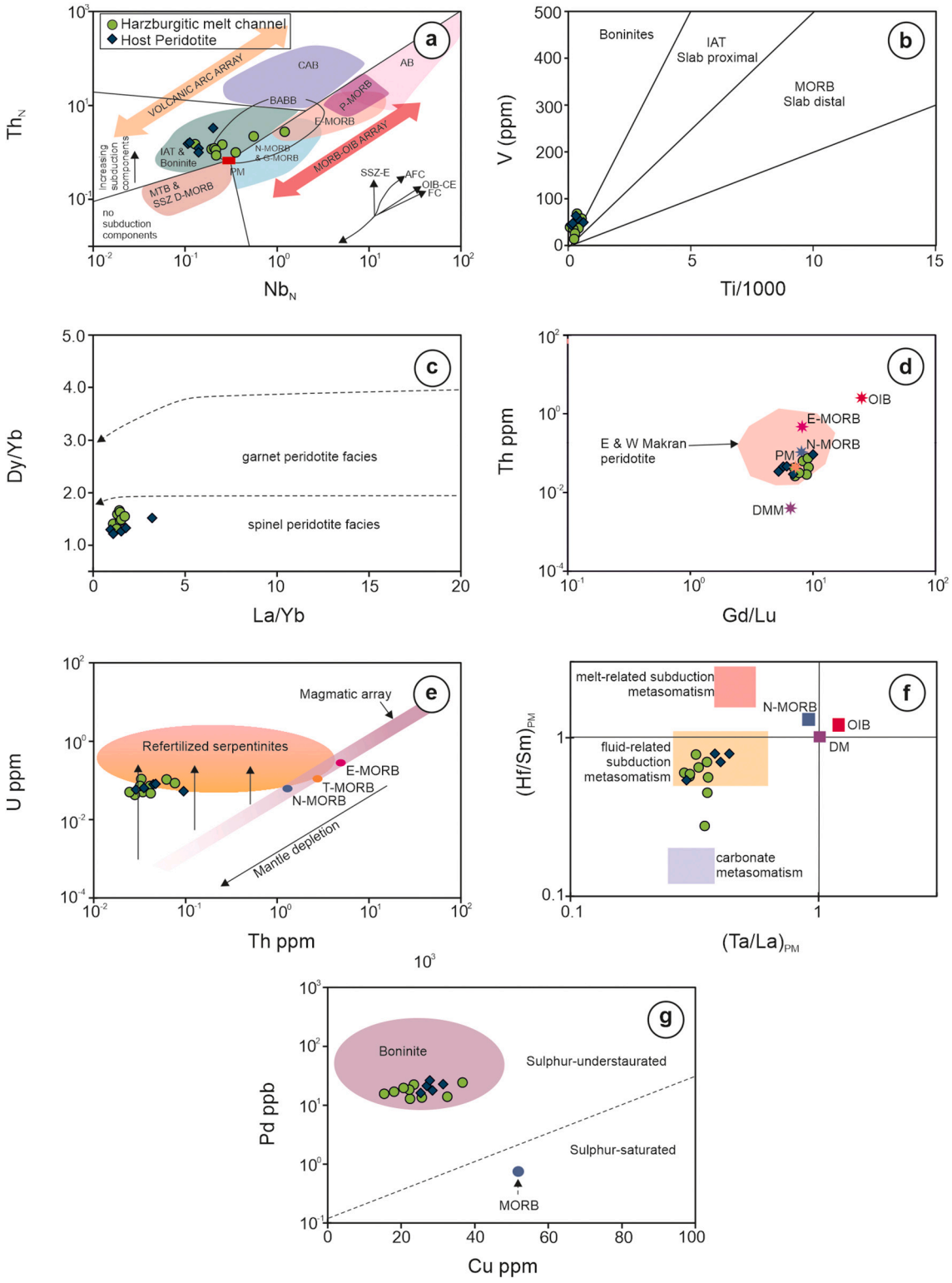

Fig. 10. (a) Th_N vs. Nb_N (after Saccani, 2015) plot showing SSZ tectonic affinity for the harzburgitic melt channels and host peridotites (b) V vs. Ti/1000 diagram illustrating the studied samples plot in distinct fields of boninite (after Shervais, 1982) (c) Dy/Yb vs. La/Yb discrimination diagram for studied peridotite samples depicting magma generation at shallower depth in spinel-peridotite stability field (after Jung et al., 2006) (d) Th ppm vs Gd/Lu diagram for studied peridotites suggesting the role of a depleted, anhydrous N-MORB mantle in their genesis (fields after Sepidbar et al., 2021) (e) U ppm vs Th ppm binary diagram adopted from Deschamps et al. (2013) showing refertilisation signatures in all the studied samples (f) $(Hf/Sm)_{PM}$ vs. $(Ta/La)_{PM}$ diagram for studied samples depicting the role of subduction derived fluid in metasomatism of harzburgitic melt channel and host peridotites (fields adopted from Deschamps et al. (2013)) (g) Pd ppb vs. Cu ppm (after Hoatson and Keays, 1989) plot exhibiting the sulphur undersaturated nature of studied harzburgite from melt channels and host.(Abbreviations: SSZ-E: supra-subduction zone enrichment; AFC: assimilation-fractional crystallization; OIB-CE: ocean island-type (plume-type) component enrichment; FC: fractional crystallization; MTB: Medium Ti basalt; MORB: mid-ocean ridge basalt, N: normal type, E: enriched type, P: plume type, G: garnet-influenced, D: depleted type; AB: alkaline basalt; IAT: island arc tholeiite, CAB: calc-alkaline basalt; BABB: backarc basin basalt; T-:Transitional type; DM: Depleted mantle; DMM: Depleted MORB mantle; PM: Primitive mantle)

Yushigou ophiolites in the North Qilian (Song et al., 2009), the Wutaishan peridotites in North China (Polat et al., 2006), and the Luobusa, Zedang and the Xigaze ophiolite in southern Tibet (Bédard et al., 2009; Bezard et al., 2011). This is in cognizance with the geochemical attributes of Andaman ophiolites, South Sandwich arc, Tso Morari massif and Izu-Bonin Mariana arc (Pearce et al., 2000; Savov et al., 2005; Deschamps et al., 2013; Saha et al., 2018). Moreover, the peridotites are marked by high Al_2O_3/TiO_2 ranging from 15.98–35.70 in conjunction with low CaO/Al_2O_3 ranging from 0.03–0.53 augmenting the role of boninitic melts in the refertilisation of the mantle wedge. Positive Eu anomalies observed in the studied melt channels indicate plagioclase fractionation under high degree of partial melting corresponding to the stability field of spinel peridotites. The positive Eu anomalies in the studied harzburgite is possibly due to enrichment and depletion events in fore arc setting and may reflect the residence time in the fore arc mantle (Parkinson et al., 1992). Similar phenomenon has been observed in the mantle peridotite recovered from Izu-Bonin-Mariana fore arc and supra subduction zone mantle peridotites from the Tethyan ophiolites of Turkey, Troodos and Pindos (Parkinson et al., 1992; Üner, 2021).

The low Ca boninitic trend for the studied rocks attested by CaO/Al_2O_3: 0.03–0.53 in conjunction with low TiO_2 contents corroborate melt extraction from an erstwhile depleted mantle refertilised by subduction-derived melts and pooling of resultant melt fractions at shallow depth (Crawford et al., 1989; Arculus et al., 1992). In coherence to this, the plots for these boninitic mantle peridotites on Th vs. Gd/Lu diagram endorse the role of a depleted, anhydrous N-MORB mantle in their genesis and similar observations have been charted for the Makran peridotites from Saudi Arabia which also depict distinct boninitic compositions (Fig. 10d) (Sepidbar et al., 2021). Nb/Yb accounts for the fertility of the mantle driven by fluids from the subducting slab. In terms of Nb/Yb and Th/Yb ratios, (Th/Yb: 0.14–0.24 for harzburgitic melt channel and 0.17–1.31 for host mantle peridotites; and Nb/Yb: 0.16–0.93 for harzburgitic melt channel and 0.10–0.68 for host mantle peridotites) the studied peridotites reflect the intervention of subduction derived component in the restitic mantle wedge (Pearce and Stern, 2006). Ba/Nb, Ba/Th and Ba/La are potent in understanding the involvement of subduction derived fluids in overprinting the refractory nature of the source. High Ba/Th (avg. 488.43 for harzburgitic melt channels and 358.91 for host rock), Ba/Nb (avg. 300.99 for harzburgitic melt channels and 485.23 for host rock) and Ba/La (avg. 60.38 for harzburgitic melt channels and 66.05 for host rock) also account for influx of slab-dehydrated fluid into the mantle. Further, higher values of Zr/Hf (host: 39.01–47.08, avg. 42.56; melt channel: 41.88–46.55, avg. 43.76) and Nd/Hf (host: 4.85–8.54, avg. 6.27; melt channel: 5.24–15.08, avg. 8.12) in conjunction with lower Nb/Ta (host: 0.19–6.89, avg. 4.49; melt channel: 5.34–17.57, avg. 11.01 excepting a lone sample with Nb/Ta: 25.02) with respect to primitive mantle values of Zr/Hf:36, Nd/Hf:4.38 and Nb/Ta:17 (Sun and Mc Donough, 1989) invoke progressive metasomatism of a depleted mantle. The studied mantle harzburgitic mantle section and melt channels of the NHO corresponding to the refertilised field above the mantle array on U vs. Th plot further conform to the phenomenon of mantle refertilisation by subduction components (Fig. 10e). The $(Hf/Sm)_{PM}$ vs $(Ta/La)_{PM}$ plot attest to fluid-driven metasomatism of mantle in a juvenile subduction zone setting. (Fig. 10f). The LILE-LREE enrichment and HFSE depletion with higher Zr/Hf, Nd/Hf and low Nb/Ta for the studied melt channels and host peridotites of NHO have been decoded in terms of metasomatic processes driven by

(i) Dehydration of Tethyan oceanic slab and release of aqueous fluids, generation of hydrous boninitic melts, low degree melting of subducted sediments carried by the Tethyan oceanic slab.
(ii) Breakdown of hydrous minerals such as mica and amphibole in the stability field of garnet and rutile.
(iii) Melting of low Mg# amphibolite in the subducting oceanic slab corresponding to the stability field of rutile.

Besides episodes of melt extraction, PGE fractionation in the mantle is governed by the degree and depth of partial melting; fractional crystallization processes and assimilation of crustal component (Arndt et al., 2005; Naldrett, 2010; Uysal et al., 2012; Manikyamba and Saha, 2014; Saha et al., 2018). The mantle peridotites in this study depict relatively higher concentrations of PGE with respect to primitive mantle values. This high concentration is ascribed to elevated abundances of IPGEs viz. Ir and Ru reflecting their refractory nature, as well as PPGEs viz. Pt and Pd reflecting further refertilisation of the refractory mantle. The mobilisation of Pd with respect to Ir (IPGE) and Pt (an element of the heavy triad) serves as clues to constrain metasomatism and refertilisation in the mantle induced by subduction-derived melts and/or fluids. PPGE/IPGE > 1 implies fluid-fluxed metasomatism. The degree of sulphur saturation in the magma can be understood from the variation of Cu with respect to Pd (Chen and Xia, 2008). Cu/Pd ranging from 1011 to 2398 for the melt channels and 1062–1595 for host mantle peridotites are lower than primitive mantle value (Cu/Pd: 7692; McDonough and Sun, 1995) substantiating sulphur undersaturation in the parental melt. Pd vs. Cu plots for the melt channels and host rocks deviate from typical S-saturated MOR composition and are consistent with S-undersaturated trend coupled with boninitic affinity (Fig. 10g). The harzburgitic melt channels and host rock peridotites from the NHO share coherent mantle traits and their petrogenetic aspects propound a transitional magmatic regime marked by refertilisation of depleted fore arc mantle by boninitic melts and slab-dehydrated fluids generated at supra subduction tectonic regime (Fig. 11). Therefore, in this case, boninitisation of a depleted, restitic upper mantle through shallow-level, flux-induced melting and melt impregnation in response to subduction initiation stands as the principal proponent for mantle refertilisation and magmatic evolution from MOR to SSZ regime (Fig. 11).

7.4. Geodynamic implications: melt migration and impregnation under SSZ regime

The mantle and crustal sections of ophiolites across the globe are intruded by dykes of diverse compositions including island arc tholeiites (IAT), alkaline basalts, boninites, gabbros, pyroxenites etc. in compliance with melt production at variable degrees and depths of partial melting of depleted and enriched mantle domains, crustal assimilation, fractional crystallization and magma chamber input. The tensile fractures or faults developed under extensional tectonic regime serve as potential pathways for melt transfer via asthenospheric diapirism, channel flow, porous flow, mantle wedge flow eventually attributing to dyke emplacement (Bonev and Stampfli, 2009; Parlak, 2016; Kavak et al., 2017; Xu et al., 2020). This significantly contributes to the emplacement, accretion and post-magmatic evolution of oceanic lithosphere. In addition to this, mantle sections of ophiolites provide unequivocal evidence for evolution of a composite lithosphere-asthenosphere system at mantle transition zone in terms of partial melting, fluid and melt influx, multistage melt migration, diffused and channelised melt flow and melt-rock interactions (Batanova et al., 2011). Melt-peridotite interaction has played a crucial role in the chemical modification of lithospheric and asthenospheric mantle during magma genesis in diverse tectonic settings. Both abyssal and SSZ peridotites have widely recorded multiple evidence for melt percolation and melt-rock interaction thereby underpinning the relevance of these processes towards the understanding of melt-migration in the oceanic mantle (Rampone et al., 2003). The geochemical features of the Mt. Maggiore ophiolitic peridotites from Corsica, France intruded by gabbro-noritic veins suggest impregnation by ascending depleted melts produced by low degree fractional melting of an ascending cold and thick lithospheric mantle column beneath slow spreading oceans (Rampone et al., 2003). Dunite and pyroxenite veins occurring within

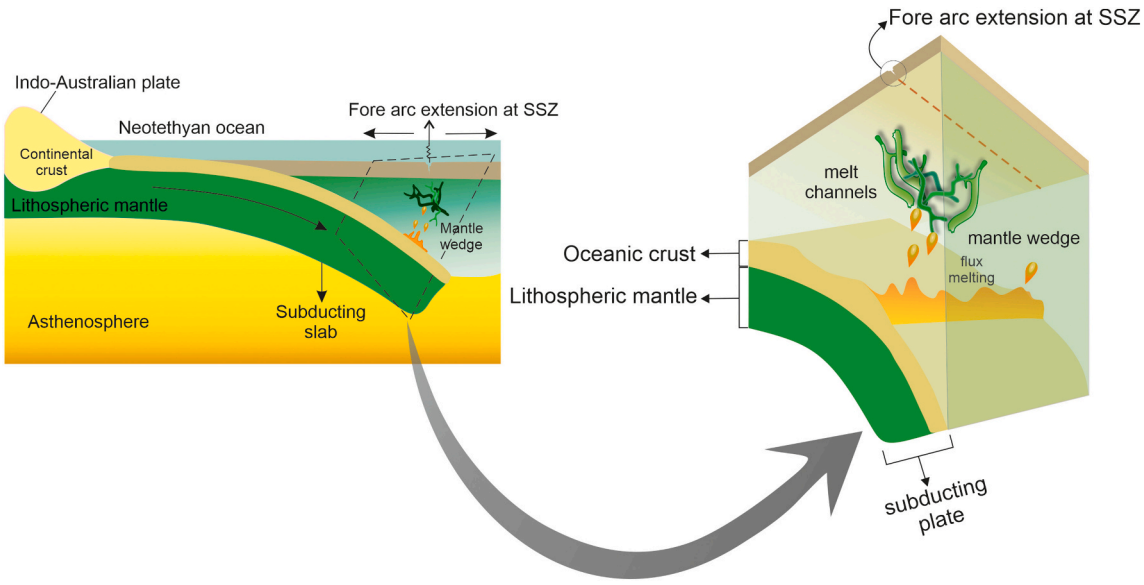

Fig. 11. Schematic tectonic model showing refertilisation of depleted mantle wedge through impregnation of boninitic melts during subduction initiation at SSZ.

host harzburgites of Voyker ophiolites from polar Urals exemplify channelized melt transport through the mantle section. The high Ca boninitic features of the percolating melts substantiate the role of slab derived melts impregnating the harzburgite and obliterating their primary composition in an open magmatic system (Batanova et al., 2011). The compositional variability observed in suprasubduction zone peridotites from Josephine ophiolite, USA and their systematic transition from depleted to fertile compositions are principally attributed to high degrees of hydrous flux melting and percolation of boninitic melts triggering mantle refertilisation (Le Roux et al., 2014).

The mantle peridotites from the NHO are interspersed with channelized melt flows that display characteristic mantle signatures and are devoid of any crustal interference. The mineral chemical attributes for the peridotites comprising the mantle section of the NHO conform to a transitional refractory MOR-type to enriched SSZ related compositional trend; however their geochemical signatures marked by V vs. Ti variations (Fig. 10b), LREE > MREE < HREE distinctly corroborate boninitic affinity. In contrast to this, the melt channels associated with these mantle peridotites of the NHO uniformly depict boninitic compositions in terms of their mineral chemistry and whole rock geochemical parameters. The boninitic imprint for the mantle peridotites and channelised melt flows thus invokes an intraoceanic subduction initiation stage featuring metasomatism and partial melting of fore arc mantle wedge with generation of boninitic melts that eventually impregnated and refertilised the mantle.

The transport of melt through the upper mantle beneath the spreading zones entails mechanisms of localisation of diffuse intergraular porous melt percolation into channel flow and reaction of migrating mantle magmas with wall peridotites resulting into formation of replacive more olivine rich counterparts (Batanova and Savelieva, 2009). The studied boninitic mantle channels can be explained by similar processes. It represents melt segregation and percolation through porous peridotitic network (Rabinowicz et al., 1987). Mantle refertilisation in SSZ regime often manifests harburgitic section with dunite, peridotite and pyroxenite channels thereby fingerprinting fluid and melt induced metasomatism, chemical heterogeneity and depleted to enriched compositional spectrum (Tollan et al., 2017). High porosity melt channels are pathways for melt migration in the mantle (Liang et al., 2010). It has been envisaged that the composition of these melt channels range from dunite to harzburgite to lherzolite and depends on the melt flux entering the channel (Liang et al., 2010). In this study, distinct mineralogical and geochemical signatures for the mantle peridotites and associated melt channels are inferred to be imparted by boninitic melts delivered by flux induced hydrous melting of an erstwhile refractory mantle in response to juvenile stages of subduction in an SSZ regime. The segregation of boninitic melts and their migration and percolation into the refertilised peridotitic mantle section of the NHO augments a 2nd stage melt migration episode in response to mantle wedge flow in a fore arc regime at a juvenile stage of subduction. The pronounced and exclusive boninitic signature for the melt channels compared to a transitional MOR-arc spectrum for their host peridotites reconciles progressive impregnation of fore arc mantle by boninitic melts concurrent with onset of subduction, dehydration and melting of Tethyan oceanic lithosphere. The boninitic composition shared by the studied melt channels and the mantle peridotites; and their spatial relation suggest that they share a common magmatic heritage and two distinct and contemporaneous stages of melt migration through the upper mantle (Python et al., 2008).

Dunitic melt channels occur as replacive features with in the mantle and are formed by the consumption of pyroxene and excess precipitation of olivine by the reactive percolation of basaltic melt through mantle peridotite. The melting of the fore arc mantle wedge in a SSZ environment results into hydrous boninitic melts which get readily evolved and saturated in orthopyroxene subsequently triggering a reverve reaction where forsterite is replaced by enstatite thereby shifting the melt composition to harzburgite. The high Mg low Ti boninitic melts carried by focused channelised flow represents proto arc and nascent arc stage of spontaneous intraoceanic subduction where the hydrous and silica rich composition of the boninitic melts allow early precipitation of orthopyroxene (Kelemen et al., 1995; Dhuime et al., 2007). Ophiolitic sequences from Chilas (Burg et al., 1998), Ladakh (Dhuime et al., 2007) and Bay of islands (Varfalvy et al., 1997) are characterised by pyroxenite dykes of boninitic affinities. Likewise, the boninitic melt channels of the NHO in this study represent the proto arc and nascent arc stages of subduction of Tethyan ocean lithosphere. The boninitic melt channels embedded within the exposed mantle section of the NHO can be translated in terms of (i) segregation of melts from the source while retaining their geochemical signatures, (ii) melt migration through interconnected channels in the host peridotites (Liang et al., 2010). In the crust-mantle transition zone and uppermost mantle, rheological condition cannot sustain focused porous flow and thus, channels are segregated between solid and melts while the latter cut across mantle peridotites. The overall mineral chemical and whole rock perspectives of the mantle peridotites and the melt channels within implicate a depleted

to enriched magma output from a heterogeneous mantle and validate a transitional geodynamic evolution of the NHO within a MOR-SSZ spectrum. The distinct LILE enrichment and LREE > MREE < HREE trend for the studied melt channels and their host are uniformly ascribed to migration and focused channelised flow of hydrated melt fractions through the oceanic mantle (McDonough and Frey, 1989; Takazawa et al., 1992; Parkinson et al., 1992).

CRediT authorship contribution statement

AV: Investigation, Data generation and processing, Methodology; Writing-original draft, AS: Conceptualization; Funding acquisition; Investigation; Methodology; Project administration, Supervision, Writing-review and editing, SG: Conceptualization, Visualization and Writing-review and editing; MS: Methodology, Formal analysis, Writing-review and editing; BD: Data generation and Writing-review and editing; MR: Data generation and Writing-review and editing.

Declaration of competing interest

The authors declare that they have no known competing financial interest or personal relationships that could have appeared to influence the work reported in this paper.

Acknowledgements

The authors are grateful to the Director, CSIR-National Institute of Oceanography for his encouragement, support and permission to publish this work. Authors are thankful to Central Analytical Facility (CAF), CSIR-NIO for extending EPMA facility. Mr. V.D. Khedekar is duly acknowledged for his kind help during EPMA data generation. MS and MR thank Director, CSIR-NGRI, Hyderabad, for support and encouragement. The authors acknowledge Dr. S.K. Verma, Editor and two anonymous reviewers for their insightful constructive comments. AS acknowledges the funding received from the Council of Scientific and Industrial Research (CSIR) and Science and Engineering Research Board (SERB), Govt. of India under MLP 2017 and GAP 3291. This is NIO's contribution no. 6805.

Appendix A. Supplementary data

Supplementary data to this article can be found online at https://doi.org/10.1016/j.chemer.2021.125821.

References

Abuamarah, B.A., 2020. Petrogenetic evolution of Cryogenian Halaban ophiolite, Saudi Arabia: a fragment of fore-arc oceanic lithosphere mantle. Lithos 356, 105303.
Abuamarah, B.A., Asimow, P.D., Azer, M.K., Ghrefat, H., 2020. Suprasubduction-zone origin of the podiform chromitites of the Bir Tuluhah ophiolite, Saudi Arabia, during Neoproterozoic assembly of the Arabian Shield. Lithos 360, 105439.
Acharyya, S.K., Ray, K.K., Roy, D.K., 1989. Tectono-stratigraphy and emplacement history of the ophiolite assemblage from the Naga Hills and Andaman island-arc, India. J. Geol. Soc. India 33, 4–18.
Acharyya, S.K., Ray, K.K., Sengupta, S., 1990. Tectonics of the ophiolite belt from Naga Hills and Andaman Islands, India. Proc. Indian Acad. Sci. (Earth Planet. Sci.) 99, 187–199.
Agrawal, O.P., Ghose, N.C., 1986. Geology and stratigraphy of the Naga Hills ophiolite between Melluri and Awankhoo, Pheek District, Nagaland, India. In: In Indian Chapter IGCP Projects 195 and 197 Meeting, pp. 163–195.
Aldanmaz, E., Koprubasi, N., 2006. Platinum-group-element systematics of peridotites from ophiolite complexes of Northwest Anatolia, Turkey: implications for mantle metasomatism by melt percolation in a supra-subduction zone environment. Int. Geol. Rev. 48, 420–442.
Aldanmaz, E., Schmidt, M.W., Gourgaud, A., Meisel, T., 2009. Mid-ocean ridge and supra-subduction geochemical signatures in spinel–peridotites from the Neotethyanophiolites in SW Turkey: implications for upper mantle melting processes. Lithos 113, 691–708.
Ali, S.A., Nutman, A.P., Aswad, K.J., Jones, B.G., 2019. Overview of the tectonic evolution of the Iraqi Zagros thrust zone: sixty million years of Neotethyan ocean subduction. J. Geodyn. 129, 162–177.
Arai, S., 1992. Chemistry of chromian spinel in volcanic rocks as a potential guide to magma chemistry. Min. Mag. 56, 173–184.
Arai, S., 1994. Characterization of spinel peridotites by olivine-spinel compositional relationships: review and interpretation. Chem. Geol. 113, 191–204.
Arai, S., Shimizu, Y., Ismail, S.A., Ahmed, A.H., 2006. Low-T formation of high-Cr spinel with apparently primary chemical characteristics within podiform chromitite from Rayat, northeastern Iraq. Min. Mag. 70, 499–508.
Arculus, R.J., Pearce, J.A., Murton, B.J., Van der Laan, S.R., 1992. Igneous stratigraphy and major element geochemistry of Holes 786A and 786B. Proc. Ocean Drill. Program Sci. Results 125, 143–169.
Arndt, N.T., 1994. Archean komatiites. In: Condie, K.C. (Ed.), Archean Crustal Evolution. Elsevier, Amsterdam, pp. 11–44.
Arndt, N.T., Lesher, C.M., Czamanske, G.K., 2005. Mantle-derived magmas and magmatic Ni-Cu-(PGE) deposits. Econ. Geol. 5–24, 100th Aniversary volume.
Balaram, V., Mathur, R., Banakar, V.K., Hein, J.R., Rao, C.R.M., Rao, T.G., Dasaram, B., 2006. Determination of the platinum–group elements (PGE) and gold (Au) in manganese nodule reference samples by nickel sulfide fire-assay and Te coprecipitation with ICP-MS. Ind. J. Geo-Mar. Sci. 35, 7–16.
Barnes, S.-J., 1990. The use of metal ratios in prospecting for platinum-group element deposits in mafic and ultramafic intrusions. J. Geochem. Explor. 37, 91–99.
Barnes, S.J., Roeder, P.L., 2001. The range of spinel compositions in terrestrial mafic and ultramafic rocks. J. Petrol. 42, 2279–2302.
Barnes, S.-J., Boyd, R., Korneliussen, A., Nilsson, L.P., Often, M., Pedersen, R.B., Robins, B., 1988. The use of mantle normalization and metal ratios in discriminating between the effects of partial melting, crystal fractionation and sulphide segregation on platinum group elements, gold, nickel, and copper: examples from Norway. In: Prichard, H.M., Potts, P.J., Bowles, S.J., Cripp, S.J. (Eds.), Geoplatinum. Elsevier, London, pp. 113–143.
Barth, M.G., Mason, P.R., Davies, G.R., Drury, M.R., 2008. The Othris Ophiolite, Greece: a snapshot of subduction initiation at a mid-ocean ridge. Lithos 100, 234–254.
Batanova, V.G., Savelieva, G.N., 2009. Melt migration in the mantle beneath spreading zones and formation of replacive dunites: a review. Rus. Geol. Geophys. 50, 763–778.
Batanova, V.G., Belousov, I.A., Savelieva, G.N., Sobolev, A.V., 2011. Consequences of channelized and diffuse melt transport in supra-subduction zone mantle: evidence from the Voykar ophiolite (Polar Urals). J. Petrol. 52, 2483–2521.
Beccaluva, L., Coltori, M., Giunta, G., Siena, F., 2004. Tethyan vs. cordilleran ophiolites: a reappraisal of distinctive tectono-magmatic features of supra-subduction complexes in relation to subduction mode. Tectonophysics 393, 163–174.
Becker, H., Horan, M.F., Walker, R.J., Gao, S., Lorand, J.P., Rudnick, R.L., 2006. Highly siderophile element composition of the Earth's primitive upper mantle: constraints from new data on peridotite massifs and xenoliths. Geochim. Cosmochim. Acta 70, 4528–4550.
Bédard, É., Hébert, R., Guilmette, C., Lesage, G., Wang, C.S., Dostal, J., 2009. Petrology and geochemistry of the Saga and Sangsang ophiolitic massifs, Yarlung Zangbo Suture Zone, Southern Tibet: evidence for an arc–back-arc origin. Lithos 113, 48–67.
Bezard, R., Hébert, R., Wang, C., Dostal, J., Dai, J., Zhong, H., 2011. Petrology and geochemistry of the Xiugugabu ophiolitic massif, western Yarlung Zangbo suture zone, Tibet. Lithos 125, 347–367.
Bhat, I.M., Ahmad, T., Rao, D.S., Balakrishnan, S., Rao, N.C., 2021. PGE and isotopic characteristics of Shergol and Suru Valley Ophiolites, Western Ladakh: implications for supra-subduction tectonics along Indus Suture Zone. Geosci. Front. 12, 101118.
Birner, S.K., Cottrell, E., Warren, J.M., Kelley, K.A., Davis, F.A., 2021. Melt addition to mid-ocean ridge peridotites increases spinel Cr# with no significant effect on recorded oxygen fugacity. Earth Planet. Sci. Lett. 566, 116951.
Bloomer, S.H., Taylor, B., Macleod, C.J., Stern, R.J., Fryer, P., Hawkins, J.W., Johnson, L., 1995. Early arc volcanism and the ophiolite problem: a perspective from drilling in the western Pacific. In: Active Margins and Marginal Basins of the Western Pacific, 88, pp. 1–30.
Bodinier, J.L., Godard, M., 2003. Orogenic, ophiolitic, and abyssal peridotites. Treat. Geochem. 2, 568.
Bodinier, J.L., Guiraud, M., Fabries, J., Dostal, J., Dupuy, C., 1987. Petrogenesis of layered pyroxenites from the Lherz, Freychinede and Prades ultramafic bodies (Ariege, French Pyrenees). Geochim. Cosmochim. Acta 51, 279–290.
Bodinier, J.L., Vasseur, G., Vernieres, J., Dupuy, C., Fabries, J., 1990. Mechanisms of mantle metasomatism: geochemical evidence from the Lherz orogenic peridotite. J. Petrol. 31, 597–628.
Bonev, N., Stampfli, G., 2009. Gabbro, plagiogranite and associated dykes in the supra-subduction zone Evros Ophiolites, NE Greece. Geol. Mag. 146, 72–91.
Bouilhol, P., Burg, J.P., Bodinier, J.L., Schmidt, M.W., Dawood, H., Hussain, S., 2009. Magma and fluid percolation in arc to forearc mantle: evidence from Sapat (Kohistan, Northern Pakistan). Lithos 107, 17–37.
Buchanan, D.L., 1988. Platinum-group Element Exploration. Elsevier, Amsterdam (200pp.).
Burg, J.P., Bodinier, J.L., Chaudhry, S., Hussain, S., Dawood, H., 1998. Infra-arc mantle-crust transition and intra-arc mantle diapirs in the Kohistan Complex (Pakistani Himalaya): petro-structural evidence. Ter. Nov. 10, 74–80.
Chen, G., Xia, B., 2008. Platinum-group elemental geochemistry of mafic and ultramafic rocks from the Xigaze ophiolite, southern Tibet. J. Asian Earth Sci. 32, 406–422.
Choi, S.H., Shervais, J.W., Mukasa, S.B., 2008. Supra-subduction and abyssal mantle peridotites of the Coast Range ophiolite, California. Contrib. Mineral. Petrol. 156, 551–576.
Crawford, A.J., Falloon, T.J., Green, D.H., 1989. Classification, petrogenesis and tectonic setting of boninites. In: Crawford, A.J. (Ed.), Boninites and Related Rocks. Unwin-Hyman, London, pp. 1–49.

Dai, J.G., Wang, C.S., Hébert, R., Santosh, M., Li, Y.L., Xu, J.Y., 2011. Petrology and geochemistry of peridotites in the Zhongba ophiolite, YarlungZangbo Suture Zone: implications for the Early Cretaceous intra-oceanic subduction zone within the Neo-Tethys. Chem. Geol. 288, 133–148.
Dale, C.W., Luguet, A., Macpherson, C.G., Pearson, D.G., Hickey-Vargas, R., 2008. Extreme platinum-group element fractionation and variable Os isotope compositions in Philippine Sea Plate basalts: tracing mantle source heterogeneity. Chem. Geol. 248, 213–238.
Deschamps, F., Godard, M., Guillot, S., Hattori, K., 2013. Geochemistry of subduction zone serpentinites: a review. Lithos 178, 96–127.
Dhuime, B., Bosch, D., Bodinier, J.L., Garrido, C.J., Bruguier, O., Hussain, S.S., Dawood, H., 2007. Multistage evolution of the Jijal ultramafic–mafic complex (Kohistan, N Pakistan): implications for building the roots of island arcs. Earth Planet. Sci. Lett. 261, 179–200.
Dick, H.J., Bullen, T., 1984. Chromian spinel as a petrogenetic indicator in abyssal and alpine-type peridotites and spatially associated lavas. Contrib. Mineral. Petrol. 86, 54–76.
Dilek, Y., Furnes, H., 2011. Ophiolite genesis and global tectonics: geochemical and tectonic fingerprinting of ancient oceanic lithosphere. Geol. Soc. Am. Bull. 123, 387–411.
Dilek, Y., Morishita, T., 2009. Melt migration and upper mantle evolution during incipient arc construction: Jurassic Eastern Mirdita ophiolite, Albania. Island Arc 18, 551–554.
Dilek, Y., Furnes, H., Shallo, M., 2008. Geochemistry of the Jurassic Mirdita Ophiolite (Albania) and the MORB to SSZ evolution of a marginal basin oceanic crust. Lithos 100, 174–209.
Eales, H.V., Reynolds, I.M., 1986. Cryptic variations within chromitites of the upper critical zone, northwestern Bushveld Complex. Econ. Geol. 81, 1056–1066.
Fischer-Gödde, M., Becker, H., Wombacher, F., 2011. Rhodium, gold and other highly siderophile elements in orogenic peridotites and peridotite xenoliths. Chem. Geol. 280, 365–383.
Franz, L., Wirth, R., 2000. Spinel inclusions in olivine of peridotite xenoliths from TUBAF seamount (Bismarck Archipelago/Papua New Guinea): evidence for the thermal and tectonic evolution of the oceanic lithosphere. Contrib. Mineral. Petrol. 140, 283–295.
Garuti, G., Fershtater, G., Bea, F., Montero, P., Pushkarev, E.V., Zaccarini, F., 1997. Platinum-group elements as petrological indicators in mafic-ultramafic complexes of the central and southern Urals: preliminary results. Tectonophysics 276, 181–194.
Ghose, N.C., Agrawal, O.P., Srivastava, S.C., 1987. Metamorphism of the ophiolite belt of Nagaland, NE India. Proc. Natl. Sem. Tert. Orog. 189–213.
Hoatson, D.M., Keays, R.R., 1989. Formation of platiniferous sulide horizons by crustal fractionation and magma mixing in the Munni Munni Layered intrusion, West Pilbara Block, West Australia. Econ. Geol. 84, 117–1804.
Jan, M.Q., Windley, B.F., 1990. Chromian spinel-silicate chemistry in ultramafic rocks of the Jijal complex, Northwest Pakistan. J. Petrol. 31, 667–715.
Jung, C., Jung, S., Hoffer, E., Berndt, J., 2006. Petrogenesis of Tertiary mafic alkaline magmas in the Hocheifel, Germany. J. Petrol. 47, 1637–1671.
Kamenetsky, V.S., Crawford, A.J., Meffre, S., 2001. Factors controlling chemistry of magmatic spinel: an empirical study of associated olivine, Cr-spinel and melt inclusions from primitive rocks. J. Petrol. 42, 655–671.
Karipi, S., Tsikouras, B., Hatzipanagiotou, K., 2006. The petrogenesis and tectonic setting of ultramafic rocks from Iti and Kallidromon Mountains, continental Central Greece: vestiges of the Pindos ocean. Can. Mineral. 44, 267–287.
Kavak, K.Ş., Parlak, O., Temiz, H., 2017. Geochemical characteristics of ophiolitic rocks from the southern margin of the Sivas basin and their implications for the inner Tauride Ocean, Central-Eastern Turkey. Geodin. Acta 29, 160–180.
Keleman, P.B., 1990. Reaction between ultramafic rock and fractionating basaltic magma I. Phase relations, the origin of calc-alkaline magma series, and the formation of discordant dunite. J. Petrol. 31, 51–98.
Kelemen, P.B., Dick, H.J., Quick, J.E., 1992. Formation of harzburgite by pervasive melt/rock reaction in the upper mantle. Nature 358, 635–641.
Kelemen, P.B., Shimizu, N., Salters, V.J., 1995. Extraction of mid-ocean-ridge basalt from the upwelling mantle by focused flow of melt in dunite channels. Nature 375, 747–753.
Kepezhinskas, P.K., Taylor, R.N., Tanaka, H., 1993. Geochemistry of plutonic spinels from the North Kamchatka Arc: comparisons with spinels from other tectonic settings. Min. Mag. 57, 575–589.
Kepezhinskas, P., Defant, M.J., Widom, E., 2002. Abundance and distribution of PGE and Au in the island-arc mantle: implications for sub-arc metasomatism. Lithos 60, 113–128.
Kharbish, S., 2020. Mineral chemistry, geochemistry, Raman spectroscopy and geotectonic significance of Neoproterozoic ophiolitic peridotites and pyroxenites from Kab Amiri district, central Eastern Desert, Egypt. Front. Sci. Res. Technol. 1, 30–45.
Khogenkumar, S., Singh, A.K., Kumar, S., Lakhan, N., Chaubey, M., Imtisunep, S., Oinam, G., 2021. Subduction versus non-subduction origin of the Nagaland-Manipur Ophiolites along the Indo-Myanmar Orogenic Belt, northeast India: fact and fallacy. Geol. J. 56, 1773–1794.
Krishna, A.K., Murthy, N.N., Govil, P.K., 2007. Multielement analysis of soils bywavelength-dispersive X-ray fluorescence spectrometry. Atom. Spectrom. 28, 202–212.
Laflèche, M.R., Dupuy, C., Bougault, H., 1992. Geochemistry and petrogenesis of Archean mafic volcanic rocks of the southern Abitibi Belt, Québec. Precam. Res. 57, 207–241.
Lambart, S., Laporte, D., Schiano, P., 2009. An experimental study of pyroxenite partial melts at 1 and 1.5 GPa: implications for the major-element composition of Mid-Ocean Ridge Basalts. Earth Planet. Sci. Lett. 288, 335–347.
Lambart, S., Baker, M.B., Stolper, E.M., 2016. The role of pyroxenite in basalt genesis: melt-PX, a melting parameterization for mantle pyroxenites between 0.9 and 5 GPa. J. Geophy. Res. Solid Earth 121, 5708–5735.
Le Roux, V., Dick, H.J.B., Shimizu, N., 2014. Tracking flux melting and melt percolation in supra-subduction peridotites (Josephine ophiolite, USA). Contrib. Mineral. Petrol. 168, 1064.
Liang, Y., Schiemenz, A., Hesse, M.A., Parmentier, E.M., Hesthaven, J.S., 2010. High-porosity channels for melt migration in the mantle: top is the dunite and bottom is the harzburgite and lherzolite. Geophy. Res. Lett. 37 https://doi.org/10.1029/2010GL044162.
Liu, T., Wu, F.Y., Liu, C.Z., Zhang, C., Ji, W.B., Xu, Y., 2019. Reconsideration of Neo-Tethys evolution constrained from the nature of the Dazhuqu ophiolitic mantle, southern Tibet. Contrib. Mineral. Petrol. 174, 1–23.
Lorand, J.P., Schmidt, G., Palme, H., Kratz, K.L., 2000. Highly siderophile element geochemistry of the Earth's mantle: new data for the Lanzo (Italy) and Ronda (Spain) orogenic peridotite bodies. Lithos 53, 149–164.
Lorand, J.P., Luguet, A., Alard, O., 2013. Platinum-group element systematics and petrogenetic processing of the continental upper mantle: a review. Lithos 164, 2–21.
Lord, R.A., Prichard, H.M., S. SÁ, J.H., Neary, C.R., 2004. Chromite geochemistry and PGE fractionation in the Campo Formoso complex and Ipueira-Medrado sill, Bahia state, Brazil. Econ. Geol. 99, 339–363.
Luguet, A., Lorand, J.P., Seyler, M., 2003. Sulfide petrology and highly siderophile element geochemistry of abyssal peridotites: a coupled study of samples from the Kane Fracture Zone (45 W 23 20N, MARK area, Atlantic Ocean). Geochim. Cosmochim. Acta 67, 1553–1570.
Manikyamba, C., Saha, A., 2014. PGE geochemistry of komatiites from Neoarchean Sigegudda greenstone terrane, western Dharwar Craton, India. In: Proceedings of the Workshop on Magmatic Ore Deposits. Geol. Soc. India Special Publ., 2, pp. 162–174.
Marchesi, C., Garrido, C.J., Harvey, J., González-Jiménez, J.M., Hidas, K., Lorand, J.P., Gervilla, F., 2013. Platinum-group elements, S, Se and Cu in highly depleted abyssal peridotites from the Mid-Atlantic Ocean Ridge (ODP Hole 1274A): influence of hydrothermal and magmatic processes. Contrib. Mineral. Petrol. 166, 1521–1538.
McDonough, W.F., Frey, F.A., 1989. REE in upper mantle rocks. In: Lipin, B., McKay, G.R. (Eds.), Geochemistry and Mineralogy of Rare Earth Elements. Mineralogical Society of America, Chelsea, Michigan, pp. 99–145.
McDonough, W.F., Sun, S.S., 1995. The composition of the Earth. Chem. Geol. 120, 223–253.
Monsef, I., Rahgoshay, M., Mohajjel, M., Moghadam, H.S., 2010. Peridotites from the Khoy Ophiolitic Complex, NW Iran: evidence of mantle dynamics in a supra-subduction-zone context. J. Asian Earth Sci. 38, 105–120.
Naldrett, A.J., 2010. Secular variation of magmatic sulfide deposits and their source magmas. Econ. Geol. 105, 669–688.
Ningthoujam, P.S., Dubey, C.S., Guillot, S., Fagion, A.S., Shukla, D.P., 2012. Origin and serpentinization of ultramafic rocks of Manipur Ophiolite complex in the Indo-Myanmar subduction zone, Northeast India. J. Asian Earth Sci. 50, 128–140.
Niu, Y., Langmuir, C.H., Kinzler, R.J., 1997. The origin of abyssal peridotites: a new perspective. Earth Planet. Sci. Lett. 152, 251–265.
O'Driscoll, B., Day, J.M., Walker, R.J., Daly, J.S., McDonough, W.F., Piccoli, P.M., 2012. Chemical heterogeneity in the upper mantle recorded by peridotites and chromitites from the Shetland Ophiolite Complex, Scotland. Earth Planet. Sci. Lett. 333, 226–237.
Ohara, Y., Ishii, T., 1998. Peridotites from the southern Mariana forearc: heterogeneous fluid supply in mantle wedge. Island Arc 7, 541–558.
Ohara, Y., Stern, R.J., Ishii, T., Yurimoto, H., Yamazaki, T., 2002. Peridotites from the Mariana Trough: first look at the mantle beneath an active back-arc basin. Contrib. Mineral. Petrol. 143, 1–18.
Palme, H., O'Neill, H.S.C., 2003. Cosmochemical estimates of mantle composition. Treat. Geochem. 2, 568.
Parkinson, I., Pearce, J.A., Thirlwall, M.E.A., Johnson, K.T., Ingram, G., 1992. Trace element geochemistry of peridotites from the Izu-Bonin-Mariana forearc, Leg 125. Proc. Ocean Drill. Program Sci. Results 125, 487–506.
Parlak, O., 2016. The tauride ophiolites of Anatolia (Turkey): a review. J. Earth Sci. 27, 901–934.
Pearce, J.A., Stern, R.J., 2006. Origin of back-arc basin magmas: trace element and isotope perspectives. Geophys. Mon.-Am. Geophys. Union 166, 63–86.
Pearce, J.A., Barker, P.F., Edwards, S.J., Parkinson, I.J., Leat, P.T., 2000. Geochemistry and tectonic significance of peridotites from the South Sandwich arc–basin system, South Atlantic. Contrib. Mineral. Petrol. 139, 36–53.
Peltonen, P., Kontinen, A., Huhma, H., 1998. Petrogenesis of the mantle sequence of the Jormua ophiolite (Finland): melt migration in the upper mantle during Palaeoproterozoic continental break-up. J. Petrol. 39, 297–329.
Pirard, C., 2010. Transfer of Melts in the Sub-arc Mantle: Insights From High-pressure Experiments and From the New Caledonia Ophiolite (Ph.D. thesis). The Australian National University.
Polat, A., Herzberg, C., Münker, C., Rodgers, R., Kusky, T., Li, J., Delaney, J., 2006. Geochemical and petrological evidence for a suprasubduction zone origin of Neoarchean (ca. 2.5 Ga) peridotites, central orogenic belt, North China craton. Geol. Soc. Am. Bull. 118, 771–784.
Python, M., Ceuleneer, G., 2003. Nature and distribution of dykes and related melt migration structures in the mantle section of the Oman ophiolite. Geochem. Geophys. Geosyst. 4 (7).

Python, M., Ceuleneer, G., Arai, S., 2008. Chromian spinels in mafic–ultramafic mantle dykes: evidence for a two-stage melt production during the evolution of the Oman ophiolite. Lithos 106, 137–154.
Rabinowicz, M., Ceuleneer, G., Nicolas, A., 1987. Melt segregation and flow in mantle diapirs below spreading centers: evidence from the Oman ophiolite. J. Geophys. Res. Solid Earth 92, 3475–3486.
Rampone, E., Hofmann, A.W., 2012. A global overview of isotopic heterogeneities in the oceanic mantle. Lithos 148, 247–261.
Rampone, E., Hofmann, A.W., Raczek, I., Romairone, A., 2003. Melt impregnation in the oceanic mantle: insights from the Mt. Maggiore (Corsica, France) ophiolitic peridotites. In: EGS-AGU-EUG Joint Assembly, p. 11019.
Rampone, E., Piccardo, G.B., Hofmann, A.W., 2008. Multi-stage melt–rock interaction in the Mt. Maggiore (Corsica, France) ophiolitic peridotites: microstructural and geochemical evidence. Contrib. Mineral. Petrol. 156, 453–475.
Rao, R.A., 1983. Geology and hydrocarbon potential of a part of Assam Arakan basin and its adjacent regions. Petrol. Asia J. 6, 127–158.
Rëhkamper, M., Halliday, A.N., Fitton, J., Alt, J., Takazawa, E., 1999. Non-chondritic platinum-group element ratios in oceanic mantle lithosphere: petrogenetic signature of melt percolation? Earth Planet. Sci. Lett. 172, 65–81.
Rollinson, H., 2008. The geochemistry of mantle chromitites from the northern part of the Oman ophiolite: inferred parental melt compositions. Contrib. Mineral. Petrol. 156, 273–288.
Rudnick, R.L., Walker, R.J., 2009. Interpreting ages from Re–Os isotopes in peridotites. Lithos 112, 1083–1095.
Saccani, E., 2015. A new method of discriminating different types of post-Archeanophiolitic basalts and their tectonic significance using Th-Nb and Ce-Dy-Yb systematics. Geosci. Front. 6, 481–501.
Saccani, E., Tassinari, R., 2015. The role of MORB and SSZ magma-types in the formation of Jurassic ultramafic cumulates in the Mirdita ophiolites (Albania) as deduced from chromian spinel and olivine chemistry. Ofioliti 40, 37–56.
Saha, A., Manikyamba, C., Santosh, M., Ganguly, S., Khelen, A.C., Subramanyam, K.S.V., 2015. Platinum Group Elements (PGE) geochemistry of komatiites and boninites from Dharwar Craton, India: implications for mantle melting processes. J. Asian Earth Sci. 105, 300–319.
Saha, A., Santosh, M., Ganguly, S., Manikyamba, C., Ray, J., Dutta, J., 2018. Geochemical cycling during subduction initiation: evidence from serpentinized mantle wedge peridotite in the south Andaman ophiolite suite. Geosci. Front. 9, 1755–1775.
Said, N., Kerrich, R., Groves, D., 2010. Geochemical systematics of basalts of the Lower Basalt Unit, 2.7 Ga Kambalda sequence, Yilgran Craton, Australia: plume impingement at a rifted Craton margin. Lithos 115, 82–100.
Salters, V.J., Stracke, A., 2004. Composition of the depleted mantle. Geochem. Geophys. Geosyst. 5 (5).
Satyanarayanan, M., Balaram, V., Sawant, S.S., Subramanyam, K.S.V., Krishna, G.V., Dasaram, B., Manikyamba, C., 2018. Rapid determination of REEs, PGEs, and other trace elements in geological and environmental materials by high resolution inductively coupled plasma mass spectrometry. At. Spectrosc. 39, 1–15.
Savov, I.P., Ryan, J.G., D'Antonio, M., Kelley, K., Mattie, P., 2005. Geochemistry of serpentinized peridotites from the Mariana Forearc Conical Seamount, ODP Leg 125: implications for the elemental recycling at subduction zones. Geochem. Geophys. Geosyst. 6 (4).
Sepidbar, F., Khedr, M.Z., Ghorbani, M.R., Palin, R.M., Xiao, Y., 2021. Petrogenesis of arc-related peridotite hosted chromitite deposits in Sikhoran-Soghan mantle section, South Iran: evidence for proto-forearc spreading to boninitic stages. Ore Geol. Rev. 136, 104256.
Shervais, J.W., 1982. Ti-V plots and the petrogenesis of modern and ophiolitic lavas. Earth Planet. Sci. Lett. 59, 101–118.
Singh, A.K., Devi, L.D., Singh, N.I., Subramanyam, K.S.V., Singh, R.B., Satyanarayanan, M., 2013. Platinum-group elements and gold distributions in peridotites and associated podiform chromitites of the Manipur Ophiolitic Complex, Indo-Myanmar Orogenic Belt, Northeast India. Geochemistry 73, 147–161.
Singh, A.K., Khogenkumar, S., Singh, L.R., Bikramaditya, R.K., Khuman, C.M., Thakur, S. S., 2016. Evidence of Mid-ocean ridge and shallow subduction forearc magmatism in the Nagaland-Manipur ophiolites, northeast India: constraints from mineralogy and geochemistry of gabbros and associated mafic dykes. Geochemistry 76, 605–620.
Song, X.Y., Keays, R.R., Zhou, M.F., Qi, L., Ihlenfeld, C., Xiao, J.F., 2009. Siderophile and chalcophile elemental constraints on the origin of the Jinchuan Ni-Cu-(PGE) sulfide deposit, NW China. Geochim. Cosmochim. Acta 73, 404–424.
Stern, R.J., Johnson, P.R., Kröner, A., Yibas, B., 2004. Neoproterozoic ophiolites of the Arabian-Nubian shield. Develop. Precambrian Geol. 13, 95–128.
Stevens, R.E., 1944. Composition of some chromites of the western hemisphere. Am. Mineral. J. Earth Planet. Mater. 29, 1–34.
Sun, S.S., Mc Donough, W.F., 1989. Chemical and isotopic systematics of oceanic basalts, implications for mantle composition and processes. In: Saunders, A.D., Norry, M.J. (Eds.), Magmatism in the Ocean Basins, Geological Society of London Special Publication, 42. Blackwell Scientific Publication, UK, pp. 313–345.
Takazawa, E., Frey, F.A., Shimizu, N., Obata, M., Bodinier, J.L., 1992. Geochemical evidence for melt migration and reaction in the upper mantle. Nature 359, 55–58.
Tollan, P.M.E., Dale, C.W., Hermann, J., Davidson, J.P., Arculus, R.J., 2017. Generation and modification of the mantle wedge and lithosphere beneath the West Bismarck island arc: melting, metasomatism and thermal history of peridotite xenoliths from Ritter island. J. Petrol. 58, 1475–1510.
Üner, T., 2021. Supra-subduction zone mantle peridotites in the Tethyan Ocean (East Anatolian Accretionary Complex–Eastern Turkey): petrological evidence for melting and melt-rock interaction. Mineral. Petrol. 34, 1–23.
Uysal, I., Tarkian, M., Sadiklar, M.B., Şen, C., 2007. Platinum-group-element geochemistry and mineralogy of ophiolitic chromitites from the Kop mountains, Northeastern Turkey. Can. Mineral. 45, 355–377.
Uysal, I., Ersoy, E.Y., Karslı, O., Dilek, Y., Sadıklar, M.B., Ottley, C.J., Meisel, T., 2012. Coexistence of abyssal and ultra-depleted SSZ type mantle peridotites in a Neo-Tethyan Ophiolite in SW Turkey: constraints from mineral composition, whole-rock geochemistry (major–trace–REE–PGE), and Re–Os isotope systematics. Lithos 132, 50–69.
Varfalvy, V., Hébert, R., Bedard, J.H., 1996. Interactions between melt and upper-mantle peridotites in the North Arm Mountain massif, Bay of Islands ophiolite, Newfoundland, Canada: implications for the genesis of boninitic and related magmas. Chem. Geol. 129, 71–90.
Varfalvy, V., Hebert, R., Bedard, J.H., Lafleche, M.R., 1997. Petrology and geochemistry of pyroxenite dykes in upper mantle peridotites of the North Arm Mountain Massif, Bay of Islands Ophiolite, Newfoundland; implications for the genesis of boninitic and related magmas. Can. Mineral. 35, 543–570.
Verencar, A., Saha, A., Ganguly, S., Manikyamba, C., 2021. Tectono-magmatic evolution of Tethyan oceanic lithosphere in supra subduction zone fore arc regime: geochemical fingerprints from crust-mantle sections of Naga Hills Ophiolite. Geosci. Front. 12, 101096.
Wang, Y.J., Hu, W.J., Zhong, H., Zhu, W.G., Bai, Z.J., 2021. Oceanic lithosphere heterogeneity in the eastern Paleo-Tethys revealed by PGE and Re–Os isotopes of mantle peridotites in the Jinshajiang ophiolite. Geosci. Front. 12, 101114.
Xu, Y., Liu, J., Xiong, Q., Su, B.X., Scott, J.M., Xu, B., Pearson, D.G., 2020. The complex life cycle of oceanic lithosphere: a study of Yarlung-Zangbo ophiolitic peridotites, Tibet. Geochim. Cosmochim. Acta 277, 175–191.
Zhou, M.F., Robinson, P.T., Malpas, J., Li, Z., 1996. Podiform chromitites in the Luobusa ophiolite (southern Tibet): implications for melt-rock interaction and chromite segregation in the upper mantle. J. Petrol. 37, 3–21.